agronomy

MDPI

Article

Regional-Scale Mapping of Gully Network in Mediterranean Olive Landscapes Using Machine Learning Algorithms: The Guadalquivir Basin

Paula González-Garrido [1,*], Adolfo Peña-Acevedo [1], Francisco-Javier Mesas-Carrascosa [2] and Juan Julca-Torres [3]

[1] ETSIAM, Civil Engineering and Engineering Projects, Department of Rural Engineering, University of Cordoba, Edif. Leonardo Da Vinci, Ctra. Madrid km 396, 14071 Cordoba, Spain; ir1peala@uco.es
[2] Department of Graphic Engineering and Geomatics, Campus de Rabanales, University of Cordoba, 14014 Cordoba, Spain; ig2mecaf@uco.es
[3] Realima Ingeniería Ambiental, Calle Aviación 59, 41007 Sevilla, Spain; jjulcatorres@gmail.com
* Correspondence: z82gogap@uco.es

Abstract

Gully erosion is a significant threat to the sustainability of soil in Mediterranean basins. Despite its impact, there is a lack of research providing accurate regional-scale cartography of complete gully networks. This study aims to automatically map the gully network in the olive-growing landscapes of the Guadalquivir basin (Spain) using Machine Learning (ML) algorithms: Random Forest (RF), Support Vector Machine (SVM), Decision Tree (DT), and Logistic Regression (LR). We integrated these models with 17 predictive variables (including hydrotopographic, climatic, and edaphic factors) and the Gully Head Initiation (GHI) index. RF was the most suitable model, achieving an Area Under the Curve (AUC) of 0.91 and an F1-score of 0.83, and enabled the delineation of a gully network totalling 8439.05 km. Variable importance analysis revealed that flow accumulation (17.33%) and the GHI index (nearly 30%) were the primary predictors, with the Rainy Day Normal (RDN)-based formulation outperforming the maximum daily precipitation (Pmax)-based one. Spatially, countryside hill landscapes exhibited the highest gully densities (42.50 m/ha). The results demonstrate the effectiveness of combining ML with physically based indices to generate high-resolution gully cartography for soil conservation planning in Mediterranean olive groves.

Keywords: erosion; olive groves; machine learning (ML); random forest (RF); gully head initiation (GHI) index; hydrotopographic variables; gully network; gully density

Academic Editors: Paul Kwan, Jing Zhou and Beibei Xu

Received: 11 February 2026
Revised: 6 March 2026
Accepted: 12 March 2026
Published: 14 March 2026

1. Introduction

Soil erosion constitutes a significant threat to environmental sustainability, agricultural productivity, and food security, as it undermines soil health and numerous associated ecosystem services. Within the European Union, it is estimated that 62% of soils are not in a healthy condition, with erosion being one of the main degradation processes, and that approximately half of agricultural land exceeds tolerable soil loss rates [1,2]. This situation has placed soil protection among the priorities of the European policy agenda, driving initiatives such as the 2023–2027 Common Agricultural Policy and other strategies linked to biodiversity and agricultural sustainability [3]. In this context, recent progress towards a common regulatory framework—including the proposal for a Soil Health Monitoring and Resilience Directive and the Nature Restoration Law—reflects the need to improve

knowledge, monitoring, and management of soil degradation processes across different spatial scales [4].

Among the different soil degradation processes, gully erosion stands out due to its high capacity to generate rapid and severe soil losses and its long-lasting impact on the landscape. In many regions worldwide, this type of erosion causes significant environmental and socio-economic consequences, including the loss of fertile soil and agricultural land, reduced productivity, increased sedimentation and siltation of reservoirs, as well as damage to infrastructure and private property [5–7]. Gully erosion has been widely recognised as one of the main causes of soil degradation and alteration of catchment hydrological functioning, and it constitutes the dominant erosive process in numerous Mediterranean and arid environments, which are particularly sensitive to surface runoff concentration [5,8–10].

This phenomenon is especially pronounced in semi-arid areas of the Mediterranean, such as Andalusia, where the combination of natural factors—physiography, climate, and edaphic characteristics—together with agricultural intensification and the absence of effective soil conservation measures has favoured the formation and expansion of gullies across extensive cultivated olive-growing areas [8,11,12]. In these contexts, early studies already indicated that gullies could contribute up to 83% of total sediment yield in Mediterranean catchments [8], results that have been confirmed by subsequent research based on detailed measurements, with estimated erosion rates ranging from 37 to 250 t ha^{-1} yr^{-1} in agricultural catchments of southern Spain [13]. Likewise, in Mediterranean agricultural landscapes, gully densities on the order of 53.3 m ha^{-1} have been documented in countryside areas, highlighting the high spatial incidence of this process [11]. In the case of olive groves in southern Spain, recent regional-scale studies have reported average densities of up to 4.75 gully heads per km^2 in the main olive-growing landscapes of the Guadalquivir Basin, evidencing the magnitude and extent of the problem within this agricultural system [14].

Gully erosion has been the subject of numerous studies over recent decades [15], given its key role in soil degradation and sediment generation. However, regional-scale assessments remain scarce [16], and soil erosion evaluations have largely focused on estimating average soil loss rates using the RUSLE (Revised Universal Soil Loss Equation) model [17,18], without adequately representing concentrated erosion processes associated with gullies. This is because such approaches only account for sheet and rill erosion, leading to an underestimation of both total soil losses and the spatial location of erosion hotspots.

Among the most widely used approaches for predicting gully initiation, the Topographic Threshold (TT) model stands out, having demonstrated good performance in identifying gully head initiation locations in numerous local-scale studies [19–23]. Nevertheless, the applicability of the TT model at broader spatial scales is limited by the high spatial and temporal variability of the factors controlling runoff generation and soil resistance. In Mediterranean agricultural olive-growing catchments, it has been shown that threshold values vary significantly between years as a function of precipitation dynamics and vegetation cover, preventing the assumption of a constant threshold across extensive areas with heterogeneous conditions [12].

In order to overcome these limitations, more explicitly process-based models have been developed, such as LANDPLANER [24] or the Gully Head Initiation (GHI) index [25]. These approaches incorporate a direct estimation of runoff using the curve number method and relate runoff shear stress to soil resistance through critical shear stress. Such models allow a more explicit representation of the physical mechanisms controlling gully initiation and offer greater potential for spatial transferability than purely empirical approaches.

In this context, the GHI index was applied in a previous study in olive groves of the Guadalquivir Basin [14], demonstrating a high capacity to differentiate between areas with

the presence and absence of gully heads, as well as some ability to distinguish between active and stable gully heads. However, this application also revealed important limitations that constrain its scope and accuracy. These include the simplified assignment of maximum precipitation in the model, based on a single value per area, which does not reflect the spatial or temporal variability of extreme events; and the restricted consideration of soil properties, focused solely on clay content for the calculation of critical shear stress, without integrating other relevant factors such as soil texture, stoniness, or soil composition [5,26,27]. In addition, the (2 × 2) m Digital Elevation Model (DEM) generated from point data, as well as the meteorological stations used, depend on data availability across the territory, which limits the scalability of the model to other areas.

Over the past decade, the use of machine learning (ML) techniques for the detection and susceptibility mapping of gully erosion has experienced remarkable growth. These artificial intelligence methodologies enable the modelling of complex, non-linear, and multivariate relationships among erosion conditioning factors, overcoming the limitations of traditional approaches [28]. For instance, ref. [29] applied four ML algorithms (Random Forest (RF), Gradient Boosted Regression Tree, Naïve Bayes Tree, and Tree Ensemble) to map gully erosion susceptibility in eastern India, achieving Area Under the Curve (AUC) values above 0.90 and demonstrating the ability of these methods to capture complex interactions among conditioning variables. In a consistent manner, ref. [28] compared different ensemble-based algorithms for regional-scale gully erosion susceptibility mapping and concluded that, in general, ensemble approaches outperform individual models in terms of both predictive performance and robustness.

Likewise, hybrid approaches integrating continental-scale inventories have been developed, such as the study by [30], which uses the European gully inventory GE-LUCAS v1.1 (3116 locations within the European Union) to derive gully erosion patterns and estimate occurrence probabilities beyond monitored locations. Taken together, these advances support the use of ML techniques as powerful tools for accurate detection and effective management of gully-affected areas. However, to date, a complete regional-scale gully network has not yet been generated; instead, studies have focused mainly on gully head locations and occurrence probabilities, as observed in continental inventories and local-scale studies.

Therefore, the main objective of this study is to automatically detect and map the gully network in the main olive-growing landscapes of the Guadalquivir River Basin using ML techniques, integrating a set of topographic, climatic, edaphic, hydrological, and spectral indices representative of vegetation cover, in order to generate robust and transferable cartography that allows the characterisation of its spatial distribution at the regional scale.

In line with this general objective, the specific objectives of the study are as follows:

- Analysis of the correlation, redundancy, and relevance of the predictive variables to select an optimal set of predictors and minimise multicollinearity issues.
- Application and comparison of different ML algorithms, assessing their ability to robustly detect the gully network and to provide a methodological framework potentially applicable to other olive-growing areas.
- Assessment of the role of the GHI index within the ML framework, incorporating it as a predictive variable in both its original formulation and an alternative formulation based on a different representation of precipitation, refining the representation of gully head initiation and activity.

2. Materials and Methods

2.1. Study Area

The study area is located within the Guadalquivir River Basin, which covers an approximate area of 57,527 km^2 (Figure 1a). The Guadalquivir basin is bordered by the Sierra

Morena mountain range to the north, the Betic mountain ranges to the south, and is developed in a south-west to north-east direction. It is also adjacent to the Atlantic Ocean. This configuration results in a marked contrast between mountainous reliefs, with elevations ranging from 1000 to 3480 m a.s.l., and the extensive central Guadalquivir valley plains, characterised by low altitudes and gentle slopes. The climate is Mediterranean of the Csa type according to the Köppen–Geiger classification [31], characterised by hot, dry summers and mild, wet winters. Mean annual temperature is approximately 16.8 °C, while mean annual precipitation reaches around 550 mm, with torrential rainfall events that may exceed 200 mm in a single day. These episodes, together with the high erodibility of the dominant clay-rich soils (Vertisols and Luvisols in lowland areas, and Cambisols and Regosols in steeper sectors), favour the development and evolution of gully erosion processes.

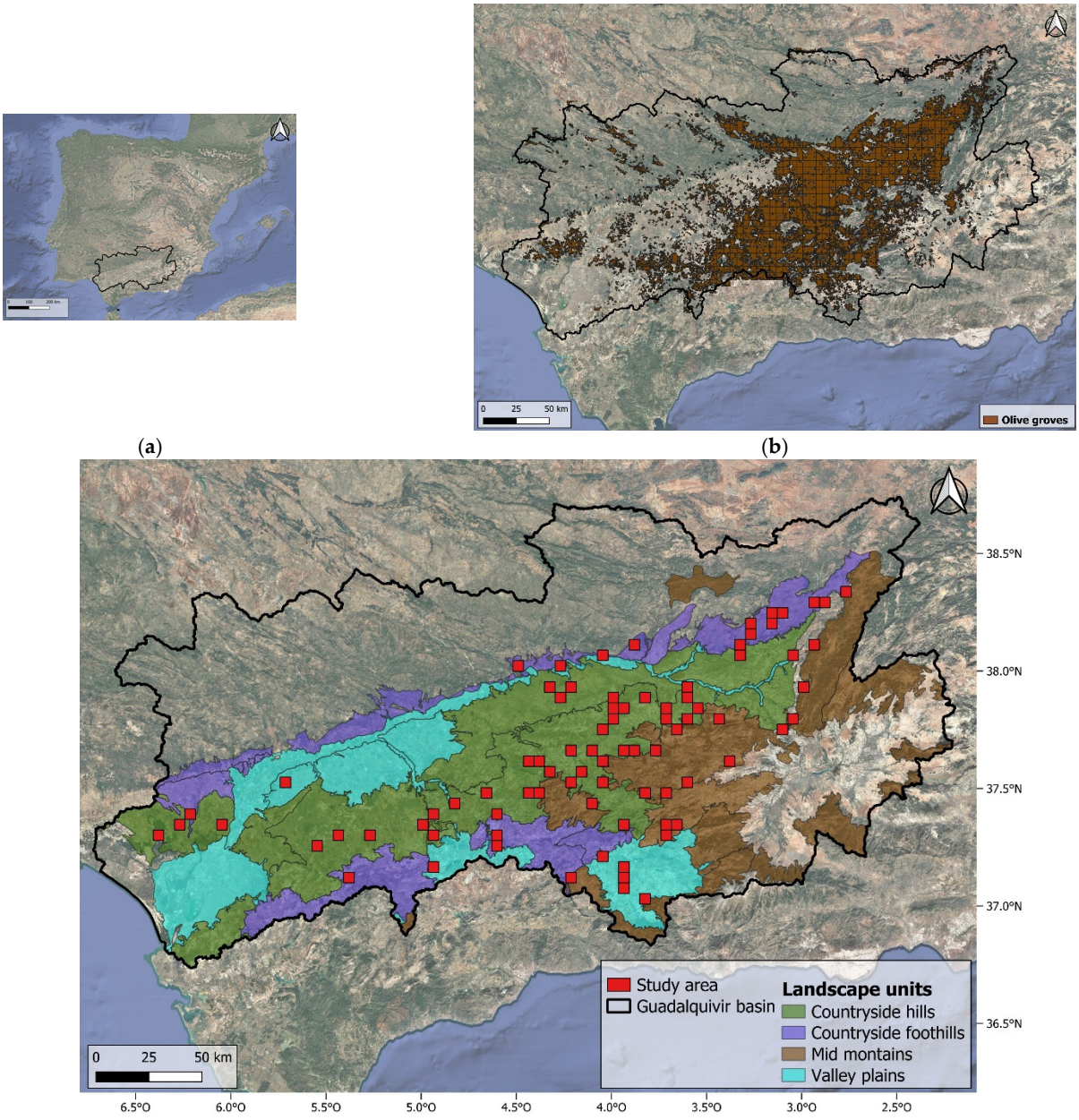

Figure 1. (**a**) Guadalquivir River basin in Andalusia (Spain); (**b**) area occupied by olive groves in Andalusia obtained from Spanish Land Use Information System (SIOSE); and (**c**) study area located in the principal landscapes units occupied by olive groves.

The Guadalquivir Basin also constitutes one of the main olive-growing regions in Europe, with more than 1.7 million hectares of olive groves [32]. The expansion of this crop, mainly on hillslopes with fragile soils, has intensified water erosion processes, with gully erosion being one of the most representative phenomena [11]. For this research, the study area was selected to represent the four main landscape units of the basin: mid-mountains, valley plains, countryside hills, and countryside foothills. The selection of these units was based on the classification of the Andalusian Environmental Information Network [33], which distinguishes landscapes according to morphological criteria, vegetation cover, and land use.

The countryside hills constitute the quintessential agricultural landscape of Andalusia. Up to 31% of the territory of the Autonomous Community of Andalusia is occupied by countryside landscapes, composed mainly of hills (over 17% of the territory) and their associated plains, forming large continuous areas historically devoted to agricultural activity. This is a highly homogeneous, robust, and strongly specialised landscape, considered one of the most representative of Andalusia. Its distinctive character is primarily due to the extensive presence of olive groves, which occupy approximately 73% of the surface area, while other rainfed and irrigated crops are confined to more limited areas [33]. From a physical perspective, these units exhibit gentle slopes (0.03–0.12 m m^{-1}) and elevations ranging between 300 and 340 m a.s.l., under a mean annual precipitation of around 565 mm. Soils are predominantly loamy-clayey, with high clay contents (≈34%) and moderate organic matter (≈1.05%), which favour the generation of concentrated runoff during intense rainfall events and condition the development of erosive processes [14].

The countryside foothills are distributed to the north and south of the Betic Depression, occupying transitional zones between this depression and the Sierra Morena and the Subbetic ranges. They are composed of hills, low ridges, and sporadic mountainous alignments, resulting in a more complex and heterogeneous relief than that of the central countryside hills. The area displays pronounced altimetric variability, dominated by low to medium-relief landforms interspersed with more prominent features, favouring a mosaic of land uses in which rainfed crops—particularly olive groves—predominate, together with shrubland and grassland areas [33]. These landscapes are characterised by steeper slopes, which may reach values of up to 0.37 m m^{-1}, and elevations between 390 and 425 m a.s.l., with lower mean annual precipitation (≈468 mm). Soils exhibit the highest clay contents (≈36%) and organic matter levels (≈1.23%) among the analysed landscapes, a combination that, together with topography, increases susceptibility to water erosion processes on cultivated hillslopes [14].

The mid-mountains form part of the extensive Andalusian mountainous domain, which represents approximately 44% of the total surface area of Andalusia. They are characterised by a moderate relief, with elevations exceeding 560 m a.s.l., while nevertheless maintaining a strong agricultural vocation. Most of the territory is devoted to rainfed agriculture, with a significant presence of olive groves and herbaceous crops adapted to more demanding topographic conditions [33]. Within the study area, these units reach elevations between 690 and 750 m a.s.l., with moderate slopes (0.05–0.31 m m^{-1}) and lower mean annual precipitation (≈435 mm). Soils exhibit sandier textures (≈42% sand) and the lowest organic matter content (≈0.98%), which results in reduced water retention capacity and a differentiated hydrological response to intense rainfall events [14].

The valley plains landscape unit occupies slightly more than 10% of the Andalusian territory. These areas develop in large depressions and wide valleys, where medium-to-high soil fertility and abundant water resources have historically supported significant agricultural production, mainly based on olive groves, together with both irrigated and rainfed herbaceous crops [33]. These landscapes are located at elevations between 370 and

430 m a.s.l., with gentle slopes (0.04–0.28 m m^{-1}) and the highest mean annual precipitation among the analysed units (592 mm). Soils present balanced textures and the highest organic matter content (1.29%) [14].

For the spatial analysis, land-use cartography from the Spanish Land Use Information System (SIOSE) was used, applying a regular grid cells of (5 × 5) km (25 km^2). In total, 1653 grid cells containing olive groves were identified within the Guadalquivir Basin (Figure 1b). In order to ensure an adequate representation of the crop and to avoid sampling areas with a residual presence of olive groves, grid cells in which olive groves covered less than 8 km^2—equivalent to slightly more than 30% of the total grid cell area—were excluded. After this filtering process, the number of potential grid cells was reduced to 725. From this subset, 87 study grid cells were finally selected (representing a total area of 2175 km^2), maintaining an equivalent sampling proportion for each landscape unit (Figure 1c). This procedure represents an approximate sampling intensity of 12% of all grid cells with an olive grove area exceeding 8 km^2.

2.2. Photointerpretation Process

The visual identification of gully points was carried out through photointerpretation using the most recent imagery available for the study area. This imagery was obtained from the National Plan for Aerial Orthophotography (PNOA), in 2022, which allowed for more accurate and up-to-date detection of active erosional forms. From the 87 study grid cells, a representative proportion was randomly selected based on the olive grove area within each landscape unit to extract these gully points for model training and validation. Once the model's performance was statistically verified, it was then applied to the remaining cells to generate the final gully network and analyze the spatial distribution of the results across the landscape units. In addition, field surveys were conducted to verify the presence and location of gullies identified through photointerpretation, thereby reinforcing the reliability of the generated inventory.

Furthermore, in order to obtain a balanced dataset for statistical analysis and model training, additional points corresponding to areas without gullies were randomly selected within the same grid cells, matching the number of identified gully heads. Moreover, unlike previous studies focused exclusively on predicting gully head points [14,16,24,25], this study also incorporated points distributed along the entire gully network, with the aim of more realistically capturing gully geometry and improving the model's ability to represent the gully network as a whole.

2.3. Geo-Environmental Predictors for Gully Network Modelling

The variables included in the model were selected based on their well-established relationship with water erosion processes and gully formation in Mediterranean agricultural environments, as documented in previous studies and discussed throughout this paper. The analysis of these variables was conducted for the period between 1 October 2019 and 15 July 2022, defined according to hydrological years, following criteria widely applied in gully erosion studies [11]. This temporal window is also consistent with the availability of the most recent cartographic data, taking as a reference the latest PNOA orthophotography available prior to the analysis period. Furthermore, the selection of this temporal interval is consistent with methodologies applied in previous studies, in which the multitemporal analysis of gully evolution was conducted using successive time windows defined according to data availability and spatial data update cycles (2008–2010, 2010–2013, and 2013–2019), thus ensuring methodological continuity with the work of [14]. Table 1 provides an overview of the variables used, together with their units, data sources, and spatial resolution, while their detailed description is presented in the following subsections.

Table 1. Overview of the model variables and their data sources.

Variables	Description	Units	Original Resolution	Source
RDN	Rainy day normal: Total annual rainfall/number of rainy days	mm/day	5 km	CHIRPS (Climate Hazards Groups Infrared Precipitation with Station data) *
Pmax	Maximum daily precipitation	mm	5 km	CHIRPS
GHI Pmax	Gully head initiation index with maximum precipitation	-	30 m	Copernicus DEM * (Digital Elevation Model)-Global and European Digital Elevation Model, REDIAM (Andalusian Environmental Information Network) and CHIRPS
GHI RDN	Gully head initiation index with rainy day normal precipitation	-	30 m	Copernicus DEM- Global and European Digital Elevation Model, REDIAM and CHIRPS
Coarse Fragment	Coarse fragment content derived from stone volume	%	500 m	ESDAC (European Soil data center) *
# Days > 13 mm	Number of days with precipitation exceeding 13 mm	Days	5 km	CHIRPS
# Days > 20 mm	Number of days with precipitation exceeding 20 mm	Days	5 km	CHIRPS
Sand content	Depth-weighted mean sand content of the soil profile	%	100 m	REDIAM
Clay content	Depth-weighted mean clay content of the soil profile	%	100 m	REDIAM
Silt content	Depth-weighted mean silt content of the soil profile	%	100 m	REDIAM
CN	Curve Number	-	20 m	REDIAM
NDVI	Normalized Difference Vegetation Index	-	10 m	ESA (European Space Agency): Copernicus Sentinel-2 *
SAVI	Soil Adjusted Vegetation Index	-	10 m	ESA: Copernicus Sentinel-2
EVI	Enhanced Vegetation Index	-	10 m	ESA: Copernicus Sentinel-2
BSI	Bare Soil Index	-	30 m	ESA: Copernicus Sentinel-2
TWI	Topographic Wetness Index	-	30 m	Copernicus DEM—Global and European Digital Elevation Model
Kns	Normalized Steepness Index	-	30 m	Copernicus DEM—Global and European Digital Elevation Model
Flow accumulation	Number of upstream cells draining into a specific pixel, representing the cumulative drainage area (A)	m^2	30 m	Copernicus DEM—Global and European Digital Elevation Model
S	Slope of the terrain expressed as the ratio between vertical elevation and horizontal distance	m/m	30 m	Copernicus DEM—Global and European Digital Elevation Model

* These layers were derived from their respective sources using the Google Earth Engine cloud computing environment.

2.3.1. Hydrotopographic Variables Derived from the DEM

This section describes a set of hydrotopographic variables derived from the Copernicus DEM that synthesise the control exerted by terrain on surface flow concentration, potential soil moisture, and the energy available for channel incision and drainage entrenchment. This product incorporates several editing processes, including water body correction, the

enforcement of a hydrologically coherent drainage network, and the editing of coastlines and other terrain structures.

To obtain slope (S, m m^{-1}) and drainage area (A, m^2), custom scripts were developed in Python 3.11 and executed within the JupyterLab 4.0.11 environment, following the theoretical framework of the D8 algorithm proposed by [34], which routes flow from each pixel to one of its eight neighbouring cells in the direction of steepest descent. This approach has been widely validated in geomorphological and hydrological studies and provides robust estimates of contributing area and S, constituting a fundamental tool for terrain analysis and the modelling of erosive processes at regional and supra-regional scales [35–37]. The relationship between these variables has been extensively used in studies to define the so-called TT for gully initiation [12,19–23,38].

Based on these same variables, a set of synthetic indices was derived to emphasise different aspects of topographic control that have proven successful in gully erosion susceptibility models [39]. The Topographic Wetness Index (TWI), originally developed by [40], is widely used to describe the influence of topography on hydrological processes, particularly soil moisture distribution and water accumulation conditions [41]. It is computed using the following expression:

$$TWI = Ln\left(\frac{A}{S}\right) \quad (1)$$

The Normalized Steepness Index (Kns) originally described by [42] is a morphometric index that allows an objective comparison of the relative steepness of different drainage segments, independently of local variations in the longitudinal profile, and relates it to the intensity of erosive processes [43]. Following the procedures established by [43], the K_{ns} index is calculated using the following expression:

$$K_{ns} = \mathrm{S} \times (\mathrm{A})^{0.45} \quad (2)$$

2.3.2. Characterization of GHI Index, Climatic Factors and Soil Properties

This section presents the primary predictors used to characterize, in an integrated manner, the hydrological and edaphic conditions controlling erosive flow generation and soil susceptibility to incision, with a particular emphasis on processes associated with gully head initiation. The GHI index, developed by [25], is based on the assumption that a gully head forms when the runoff shear stress exceeds the critical shear stress of the soil [44]:

$$\tau > \tau_{cr} \quad (3)$$

where τ is the runoff shear [Pa] and τ_{cr} is the critical shear stress of the soil [Pa]. The runoff shear stress is calculated using the following equation [45]:

$$\tau > \rho g R S \quad (4)$$

where ρ represents the water density [kg/m^3], g the gravity constant [N/kg], R the hydraulic radius [m] and S the local slope [m/m].

R is difficult to determine, as the channel width and flow depth are typically unknown; however, both are proportional to the peak runoff discharge [46]. In this study, the Curve Number (CN) method is used to obtain the runoff depth [47]:

$$R_d = \frac{(\mathrm{P} - \lambda S_\lambda)^2}{\mathrm{P} + (1 - \lambda) S_\lambda} \quad (5)$$

where *Rd* is the daily runoff depth, *P* is the daily rainfall depth (mm) y the maximum potential runoff losses, where λ is the initial extraction fraction. The environmental factors upon which the CN depends are combined to estimate S_λ [47]:

$$S_{0.05} = 33.96\left(\frac{100}{NC - 10}\right) \quad (6)$$

Subsequently, by multiplying R by the drainage area A [m^2], the daily discharge volume Q [m^3] is obtained. Q is used as a proxy for the hydraulic radius (R) and, by omitting the constants ρ and g, the Shear Stress (SSI) index is derived. This index provides a simplified relationship with the shear stress (τ):

$$SSI = Q \times S \quad (7)$$

On the other hand, the Critical Shear Stress (*CSI*) index is calculated using an expression based on the clay percentage [48]:

$$CSI = 0.311 \times 10^{0.0182Pc} \quad (8)$$

where *Pc* is the clay percentage at each point analyzed in the study. Finally, by combining Equations (7) and (8), the *GHI* index is obtained:

$$GHI = \frac{SSI}{CSI} \quad (9)$$

The resulting index is an empirical and dimensionless indicator, where higher values denote areas more susceptible to erosion and gully formation.

A primary limitation identified in previous studies was the exclusive use of maximum precipitation (Pmax) as the pluviometric variable [14]; therefore, in this work, the GHI is incorporated into the model both in its traditional formulation and in an alternative formulation. This alternative version includes the Rainy Day Normal (RDN) parameter [49] instead of Pmax to represent rainfall intensity. This variable has proven to be an effective descriptor of the temporal variability TT for gully initiation, as it explains changes in the erosion resistance coefficient (k) associated with interannual rainfall conditions [12].

Furthermore, to assess their independent contribution to the composite index, clay content, CN, Pmax, and RDN are included as independent explanatory variables in the model.

Additionally, two further rainfall-related hydrological variables were incorporated due to their direct influence on erosive processes. First, the number of days with precipitation exceeding 13 mm (P > 13 mm) was considered, a threshold defined as the minimum rainfall capable of generating significant erosive effects [50]. Second, a variable based on the number of days with precipitation exceeding 20 mm (P > 20 mm) was included, as this represents a critical threshold for gully development in clayey agricultural soils [5].

Specifically, clay content and CN are incorporated as static layers with unique values per pixel, while the hydrological variables are derived from the CHIRPS precipitation series corresponding to the entire analysis period (2019–2022).

2.3.3. Spectral Indices for Vegetation Cover Characterization

This section integrates spectral predictors to characterise surface erosive dynamics through the state of vegetation cover, as it is a critical factor in regulating surface runoff and protecting the soil against rainfall impact, thereby acting as a control mechanism against sheet and rill erosion [51]. In addition, several studies have demonstrated the relevance of spectral indices such as the Normalized Difference Vegetation Index (NDVI), Soil-Adjusted

Vegetation Index (SAVI), Enhanced Vegetation Index (EVI), and Bare Soil Index (BSI) for modelling soil susceptibility to erosion and gully formation [39,52,53].

Spectral indices were computed using Sentinel-2 imagery from the European Space Agency (ESA), acquired by the Sentinel-2A and Sentinel-2B satellites, which provide multispectral information across 13 bands, with spatial resolutions of up to 10 m and an approximate revisit frequency of five days. In this study, Level-2A products were used, which include atmospheric correction and allow direct use of surface reflectance values from imagery accessed and processed through the Google Earth Engine platform. Furthermore, in order to adequately represent vegetation conditions during periods when erosive processes may occur, spectral index values were calculated as the median of the image closest to the most intense precipitation events exceeding 13 mm identified during the study period.

2.4. Spatial Processing of Predictor Variables and Multicollinearity Assessment

Once generated, all variables were integrated as continuous raster layers, with each pixel representing the corresponding value within the study grid cells for the period October 2019–July 2022. Depending on their nature, these layers represent maximum, mean, or accumulated conditions over the analysis period, or static descriptors with a single value per pixel derived directly from non-temporal cartographic sources, such as the DEM or soil properties.

All data processing was conducted in the JupyterLab 4.0.11 environment using the Python 3.11 programming language. Spatial layers were first reprojected to the ETRS89/UTM Zone 30N coordinate reference system (EPSG: 25830) to ensure precise spatial alignment. The raster layers were then clipped to the boundaries of the study grid cells, retaining only the information corresponding to the area of interest.

Because spectral indices provide the highest spatial resolution among the predictors used in the model (10 m), this resolution was adopted as the reference. Accordingly, all remaining variables, originally available at coarser spatial resolutions (20 m, 30 m, 100 m, 500 m and 5 km), were resampled to this resolution. This procedure ensured spatial coherence across all predictor layers and avoided artefacts associated with the integration of heterogeneous spatial resolutions.

After spatial harmonisation, multicollinearity among predictor variables was assessed using two statistical indicators: the tolerance (TOL) and the Variance Inflation Factor (VIF). These metrics were used to identify potential redundancy and linear dependence, thereby improving the stability and predictive performance of the ML models [29,54–56]. The VIF is calculated as

$$TOL = 1 - \mathrm{Rj}^2 \tag{10}$$

$$VIF = \frac{1}{(1 - \mathrm{Rj}^2)} \tag{11}$$

where Rj^2 is the coefficient of determination of the regression of variable j against the remaining predictors. Variables with VIF values ≥ 10 and a TOL < 0.1 were considered problematic [57,58] and were excluded from the final set of predictors to ensure a more robust model.

Once redundant variables were removed based on the VIF and TOL thresholds, the relationships among the remaining predictors were further explored through a Pearson correlation analysis. This coefficient is used to measure the strength of the relationship between pairs of variables. It ranges from -1 to 1, with values close to ± 1 indicating strong associations and values near 0 indicating no correlation [59].

2.5. Modeling the Current Gully Network

The modelling of the current gully network was conducted using a ML approach, a branch of computer science applied to data analysis and classified as a form of artificial intelligence, as it enables computers to learn from experience in a manner analogous to humans or animals [60]. ML techniques rely on computational methods to capture the relationship between predictors and target variables without relying on a predefined equation-based model [61], which makes them particularly suitable for addressing non-linear problems involving large, multi-source datasets [62].

In this study, a supervised learning approach was adopted, in which the model is trained using known input data and their corresponding outputs to establish a predictive rule [60]. The main objective of this process is to map a set of explanatory or predictive variables ($x = \{x_1, \ldots, x_n\}$) to an output or response variable (y) through training samples, thereby deriving an approximate function f(x) that minimises the error between observed and predicted values [61].

Under this supervised learning framework, the modelling was performed using four classification algorithms: LR, SVM, DT, and RF. A stratified 10-fold cross-validation with three repetitions was applied to all algorithms to ensure a robust assessment of model performance. This procedure allowed the comparison of the different models and the selection of the algorithm with the highest predictive capability based on accuracy, precision, sensitivity (recall), F1-score, and the AUC. Once the best algorithm was selected, a binary raster (representing gully and non-gully areas) and a vector gully network were obtained.

The complete workflow—including data preprocessing, algorithm training, cross-validation, performance metric computation, and variable importance analysis—was implemented in the Python programming language using the specialised Scikit-learn library [63].

2.5.1. Machine Learning Algorithms for Gully Detection

Several supervised classification algorithms were evaluated in order to identify the model with the best performance for gully detection. The selection of these algorithms was based on their proven effectiveness in erosion-related studies; authors such as [64] have highlighted the suitability of RF, SVM, and DT algorithms for this purpose.

The RF algorithm was selected due to its high stability and its ability to capture non-linear relationships without the need for prior parameter elimination [65]. This ensemble algorithm combines multiple DT to reduce variance, improve generalisation, and enable the estimation of variable importance [66]. SVM is particularly effective in the analysis of complex geo-environmental problems, as it is relatively insensitive to noise in the input data and operates by identifying the optimal hyperplane that maximises the margin between classes, while addressing non-linear relationships through kernel functions [67,68].

Finally, algorithms such as LR and DT have demonstrated high predictive accuracy in gully susceptibility mapping, enabling the definition of clear rules for the identification of erosion areas [69]. LR estimates the probability of class membership through a sigmoid function, standing out for its interpretability [70], whereas DT partition the predictor space into homogeneous regions, enhancing model clarity [71].

2.5.2. Model Validation and Performance Assessment

The dataset was initially divided into a training subset (70%) and an independent test subset (30%) using a spatial stratified sampling approach. This method ensured that training and testing samples were selected from distinct geographical areas to minimize spatial autocorrelation and guarantee a truly independent evaluation. Subsequently, a repeated stratified 10-fold cross-validation was applied to the training set with three repetitions. This procedure enabled the results from multiple random partitions to be

averaged, thereby reducing variance and providing a robust estimate of model performance prior to the final evaluation on the independent test dataset [72].

In order to assess the performance of the ML algorithms, a confusion matrix was computed. This tool employs a comparative analysis of model predictions and observed values across four fundamental categories: true positives (TPs), false negatives (FNs), false positives (FPs), and true negatives (TNs) [73]. Based on these outcomes, several statistical metrics were calculated (Table 2), enabling a comprehensive and accurate evaluation of the classification models [70]. These include accuracy, which represents the total proportion of correctly classified cases; and sensitivity (also referred to as recall), which indicates the ability to detect actual positives. Furthermore, precision was calculated as the fraction of positive predictions that were correct, along with the F1-score, which provides a balance by using the harmonic mean of precision and recall, offering a robust assessment in the context of class-imbalanced gully datasets.

Table 2. Statistical metrics derived from the confusion matrix (TP = true positive, FN = false negative, FP = false positive, and FN = false negative).

Metric	Formula
Accuracy	$\frac{TP+TN}{TP+TN+FP+FN}$
Precision	$\frac{TP}{TP+FP}$
Sensitivity (recall)	$\frac{TP}{TP+FN}$
F1-score	$2 \times \frac{precision \times recall}{precision+recall}$
FCR (False Classification Rate)	$\frac{FP+FN}{TP+FP+FN}$

Additionally, the Area Under the Curve (AUC) was employed as a fundamental parameter to assess the overall performance of the classification models. The AUC provides a robust measure of the model's ability to discriminate between classes—for instance, distinguishing between gully and non-gully areas [74]. The closer the AUC value is to 1, the higher the predictive power of the model, with a value of 1 representing a perfect classification and 0.5 suggesting performance equivalent to a random guess [74,75]. Finally, the False Classification Rate (FCR) was incorporated to quantify the concentration of failures among positive instances, providing stakeholders and soil conservation planners with a direct percentage representing operational risk [76].

2.5.3. Variable Importance Analysis

Once the best-performing algorithm had been selected, an assessment of predictor importance was conducted. This analysis allows the identification of the most relevant predictors for modelling the gully network, as variables that contribute substantially to model performance have a direct influence on the accuracy of its predictions [77].

The importance of each predictor was quantified using the Mean Decrease in Impurity (MDI), a measure based on the Gini impurity reduction. This approach, derived from tree-based algorithms developed by [78], measures the total reduction in data heterogeneity (node impurity) achieved through splits based on a given variable throughout the model structure [66]. To facilitate interpretation, importance values were normalised and represented as a percentage-based importance plot, allowing predictors to be ranked according to their relative contribution to the model's predictive capability. Furthermore, a correlation analysis was conducted between gully occurrence and the most pertinent environmental predictors, with a view to investigating their statistical relationship.

2.5.4. Generation of the Current Gully Network

Finally, the current gully network was generated through pixel-based classification, where each cell was assigned as either gully presence or absence. During the processing stage, areas corresponding to roads and the official hydrographic network were masked in order to avoid misclassification with gully networks. This step was implemented to minimise false positives derived from linear infrastructures or permanent fluvial channels. Before the vectorisation process was implemented, a specific post-processing step was applied to the binary raster. This step was essential for reducing noise in the classification process and enhancing the continuity of the structure. Firstly, a binary dilation was implemented using 8-neighbour connectivity (3×3 window) in order to close single-pixel gaps and enhance local connectivity between adjacent classified pixels. Secondly, a connected-component size filtering was performed, removing clusters smaller than 3 pixels (equivalent to 300 m^2 at 10 m resolution) to suppress isolated artefacts. Finally, a skeletonization procedure was applied to reduce the binary gully areas to a one-pixel-wide medial axis while preserving topological connectivity. This step ensured geometric consistency and prevented the thickening of linear features during vectorisation.

The resulting binary raster was automatically vectorised based on the spatial connectivity of adjacent pixels by linking the centroids of gully-classified pixels, thereby transforming the raster structure into a continuous network of linear features (LineStrings). Subsequently, total gully length and gully density (m ha^{-1}) were calculated for each landscape type.

All processing was performed in block-wise mode using the Rasterio library, enabling the handling of large datasets without exceeding system memory. As a result, both a categorical raster layer and a unified vector layer of the gully network were produced, providing an operational tool for spatial assessment of erosion risk and territorial planning.

3. Results

3.1. Gully Inventory and Spatial Distribution

The gully inventory used in this study comprises a total of 1226 points, including gully heads and points distributed along gully channels, across four landscape units. Of these, 532 points were field-surveyed to validate the identification derived from photointerpretation of the 2022 PNOA orthophotography (Table 3; Figure 2). To balance the dataset, 1200 non-gully points were randomly selected, ensuring a balance proportion between classes. The field validation process entailed more than simply confirming the presence of isolated gully head points. During field visits, the gully segments were inspected along their length to verify that the photointerpreted points formed part of a continuous and morphologically coherent linear incision. This procedure allowed us to confirm not only the positional accuracy of individual points but also the structural continuity of the associated gully segments, providing an additional empirical validation of the generated network geometry.

Table 3. Number of photointerpreted and field-surveyed gully points.

Landscape Unit	Number of Gully Points Photointerpreted	Number of Gully Points Field-Surveyed
Countryside foothills	208	75
Countryside hills	722	292
Valley plains	134	89
Mid-mountains	162	76
Total	1226	532

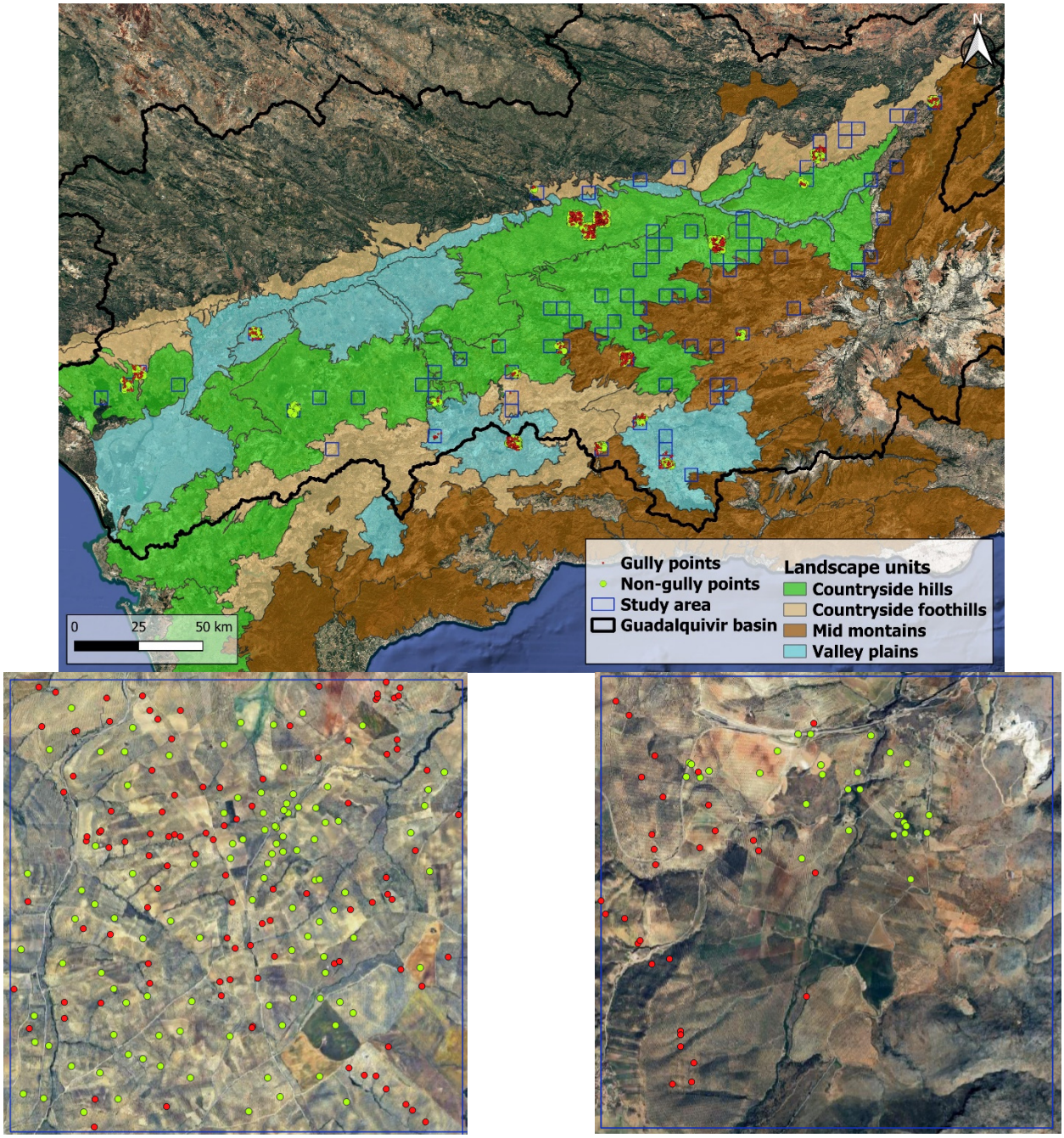

Figure 2. Study area within the Guadalquivir River basin and spatial distribution of gully and non-gully points across landscape units. The bottom panels show detailed of countryside hills and mid-mountains (**left**) and countryside foothills (**right**).

3.2. Final Predictor Set

Multicollinearity analysis enabled the refinement of the predictor set by identifying redundant variables. In this process, Kns and SAVI were excluded for exceeding the established limits (VIF > 10 and TOL < 0.1).

Following the removal process, the final set of predictors consisted of the following variables: RDN, Pmax, number of days with precipitation >13 mm and >20 mm, GHI index (GHI Pmax and GHI RDN), soil properties (sand, silt, clay, coarse fragment content, and curve number), topographic variables (S, flow accumulation and TWI), and indices describing vegetation cover and soil surface conditions (NDVI, EVI and BSI). The final

predictor set ensures an adequate level of independence among variables and constitutes the basis for model training.

Finally, a Pearson correlation matrix was constructed for the set of 17 predictors to summarise the pairwise associations (see Figure 3). Overall, the majority of the correlations were weak ($r < 0.40$), with only a limited number of moderate-to-strong relationships. Significant positive correlations were identified among rainfall-related variables, including # Days > 13 mm and # Days > 20 mm ($r = 0.71$), Pmax with RDN ($r = 0.74$), and RDN with # Days > 20 mm ($r = 0.73$). The two GHI formulations demonstrated a strong correlation ($r = 0.74$). Soil properties were analysed, and it was found that clay and sand content showed a marked negative association ($r = -0.56$), while silt and clay content were moderately correlated ($r = 0.42$). With regard to spectral indices, the NDVI and EVI were found to be positively correlated ($r = 0.71$), and both demonstrated strong negative correlations with BSI ($r = -0.72$ for both).

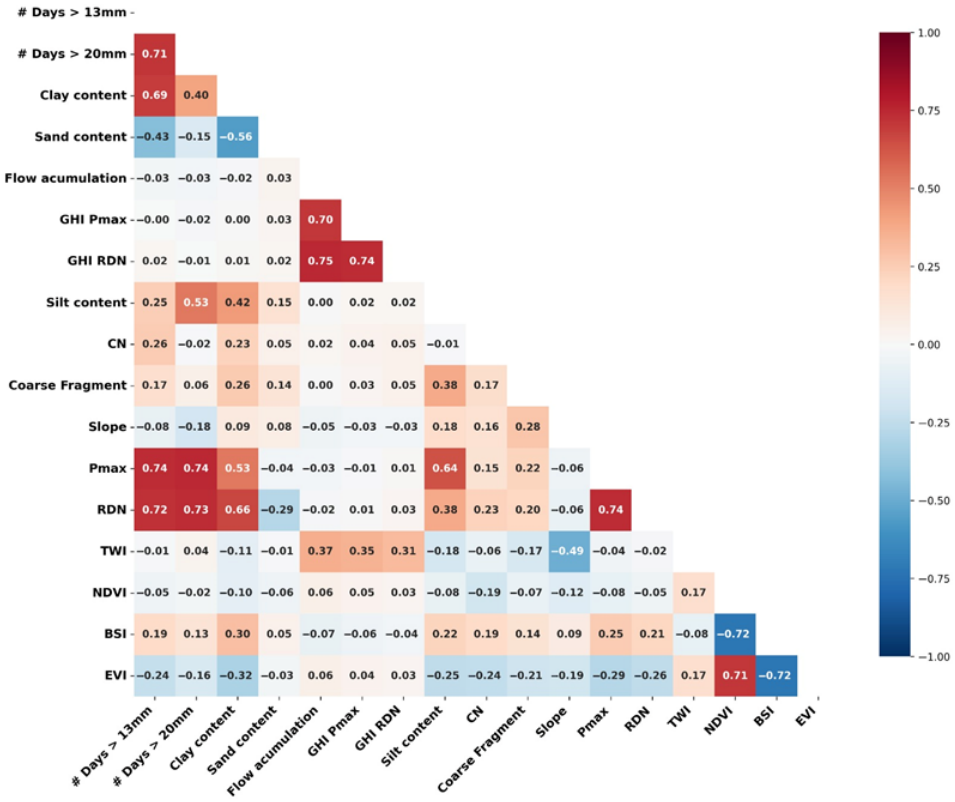

Figure 3. Pearson's correlation matrix among the final set of 17 predictor variables, including hydrotopographic, climatic, and soil-related factors.

3.3. Model Selection and Performance Comparison

As shown in Table 4, the best-performing models were RF and SVM, followed by DT and LR. In particular, RF achieved the highest values for F1-score (0.8347), accuracy (0.8259), recall (0.8549), and AUC (0.9135), indicating a well-balanced performance in terms of predictive capability and sensitivity Furthermore, the RF model exhibited the lowest False Classification Rate (FCR = 0.1631), which represents a significant reduction in operational risk compared to the other algorithms evaluated.

SVM also demonstrated competitive performance, with AUC (0.8092) and accuracy (0.7266) values, although these were lower than those obtained by RF. In contrast, LR demonstrated comparatively poorer performance, particularly in terms of recall (0.6609), which was the lowest among the evaluated models. The DT model also recorded overall metrics below 0.80 for most indicators.

Table 4. Performance evaluation of the ML models.

Algorithm	F1-Score	Accuracy	Precision	Recall	AUC	FCR
Random Forest (RF)	0.8347	0.8259	0.8163	0.8549	0.9135	0.1631
Decision tree (DT)	0.7736	0.7674	0.7748	0.7737	0.7672	0.2422
Support vector machine (SVM)	0.7348	0.7266	0.7337	0.7368	0.8092	0.3145
Logistic regression (LR)	0.7261	0.7440	0.8069	0.6609	0.8129	0.2911

Although SVM achieved competitive results, RF clearly provided the best overall balance between accuracy, detection capability, and robustness, yielding the highest values across all evaluation metrics considered. Consequently, RF was selected as the most robust model for the gully network generation.

3.4. Variable Importance Assessment

The results of the relative importance of the predictor variables, derived from the RF model (Figure 4), indicate that the variables exerting the strongest influence on gully prediction are primarily related to hydrological and topographic dynamics. Specifically, flow accumulation emerges as the most influential predictor, contributing 17.33% to the model, followed by the GHI–RDN (14.63%) and GHI–Pmax (14.00%). Taken together, both GHI formulations account for nearly 30% of the total model importance. These three variables collectively explain approximately 46% of the overall importance.

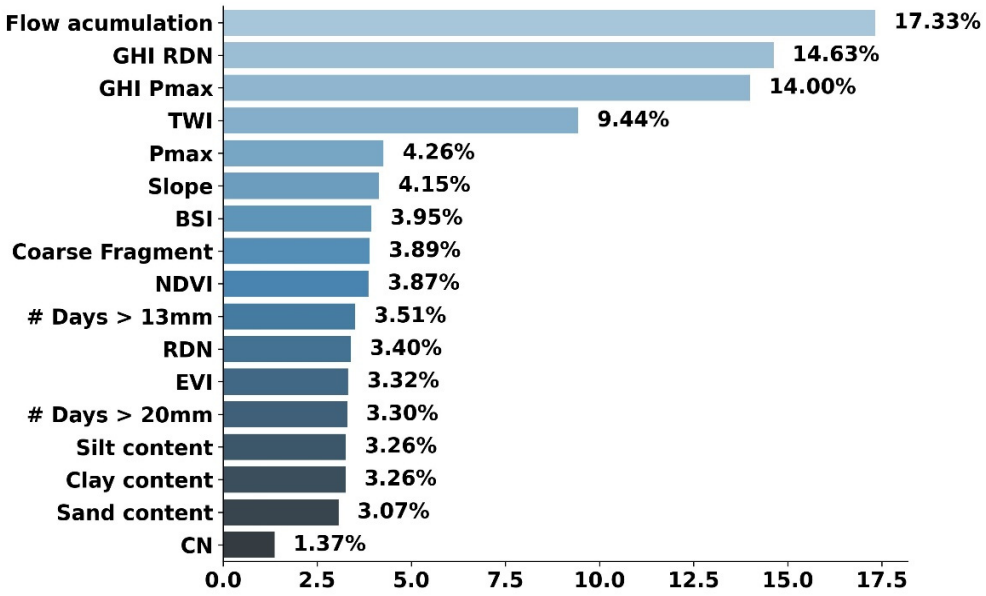

Figure 4. Relative importance (%) of predictor variables in the Random Forest (RF) model.

The TWI also exhibits a substantial contribution (9.44%), reinforcing the relevance of soil saturation conditions and topographic control over moisture distribution. The four most influential variables represent approximately 55% of the total model importance, indicating that a significant proportion of the predictive performance is governed by hydrotopographic factors.

A second group of variables, with individual contributions ranging between 3.5% and 5%, includes Pmax, S, BSI, coarse fragment, and the NDVI. Despite their individual influence being lower, these variables provide complementary information related to vegetation cover status, and surface soil properties, which modulate landscape responses to erosive processes.

Climate-related variables based on precipitation thresholds (number of days exceeding 13 mm and 20 mm, as well as RDN) and soil textural properties (sand, silt, and clay content)

exhibit individual contributions below 3.5%, acting as secondary factors in the spatial discrimination of gully presence. The CN demonstrates the lowest contribution (1.37%), suggesting a limited influence within the context of the developed model.

The correlation analysis between gully occurrence and the selected environmental predictors (see Table 5) revealed two distinct patterns based on the nature of the variables. The primary hydrotopographic predictors demonstrated a positive correlation with gully presence, specifically flow accumulation (r = 0.70), the GHI RDN index (r = 0.63), TWI (r = 0.62), and GHI Pmax (r = 0.57). In contrast, the vegetation indices demonstrated a negative correlation, with values of r = −0.25 for EVI and r = −0.19 for NDVI. All correlation coefficients for these predictors were statistically significant, confirming the consistency of these relationships across the study area.

Table 5. Pearson correlation coefficients (r) and significance levels (*p*-values) between gully occurrence and selected environmental predictors.

Variable	r	*p*-Value
GHI RDN	0.63	2.1×10^{-12}
GHI Pmax	0.57	4.3×10^{-11}
Flow accumulation	0.70	6.5×10^{-13}
TWI	0.62	3.7×10^{-12}
NDVI	−0.19	5.2×10^{-3}
EVI	−0.25	2.8×10^{-3}

3.5. Spatial Distribution of the Generated Gully Network

The selected model enabled the generation of gully network mapping through a binary pixel-based classification, distinguishing between areas with and without gully presence. The total gully length and gully density were measured for each landscape type, based on the generated network (Table 6). The results indicate a total gully length of 8439.05 km, with the highest density recorded in the countryside hills at 42.50 m ha^{-1}. Comparable values are observed in the countryside foothills, with a density of 40.10 m ha^{-1}, indicating a high susceptibility to gully formation and development in both landscapes. In contrast, mid-mountains areas show a substantially lower gully density (31.43 m ha^{-1}), which may be related to steeper slopes combined with lower continuous surface flow concentration. Similarly, valley plains exhibit moderate gully densities (30.58 m ha^{-1}), reflecting an intermediate geomorphological response.

Table 6. Gully network length and density by landscape unit.

Landscape Unit	Gully Network Length, km	Gully Network Density, m/ha^{-1}
Countryside hills	4887.72	42.50
Countryside foothills	1684.15	40.10
Mid-mountains	1178.98	31.43
Valley plains	688.2	30.58

Figure 5 illustrates examples of the generated gully network for each analysed landscape type. The maps clearly reveal distinct differences in the spatial distribution and concentration of gullies as a function of the geomorphological and topographic characteristics of each landscape unit. Overall, the gully network exhibits greater density and continuity in the countryside landscapes, whereas in mid-mountain areas and valley plains, the gully network appears less dense.

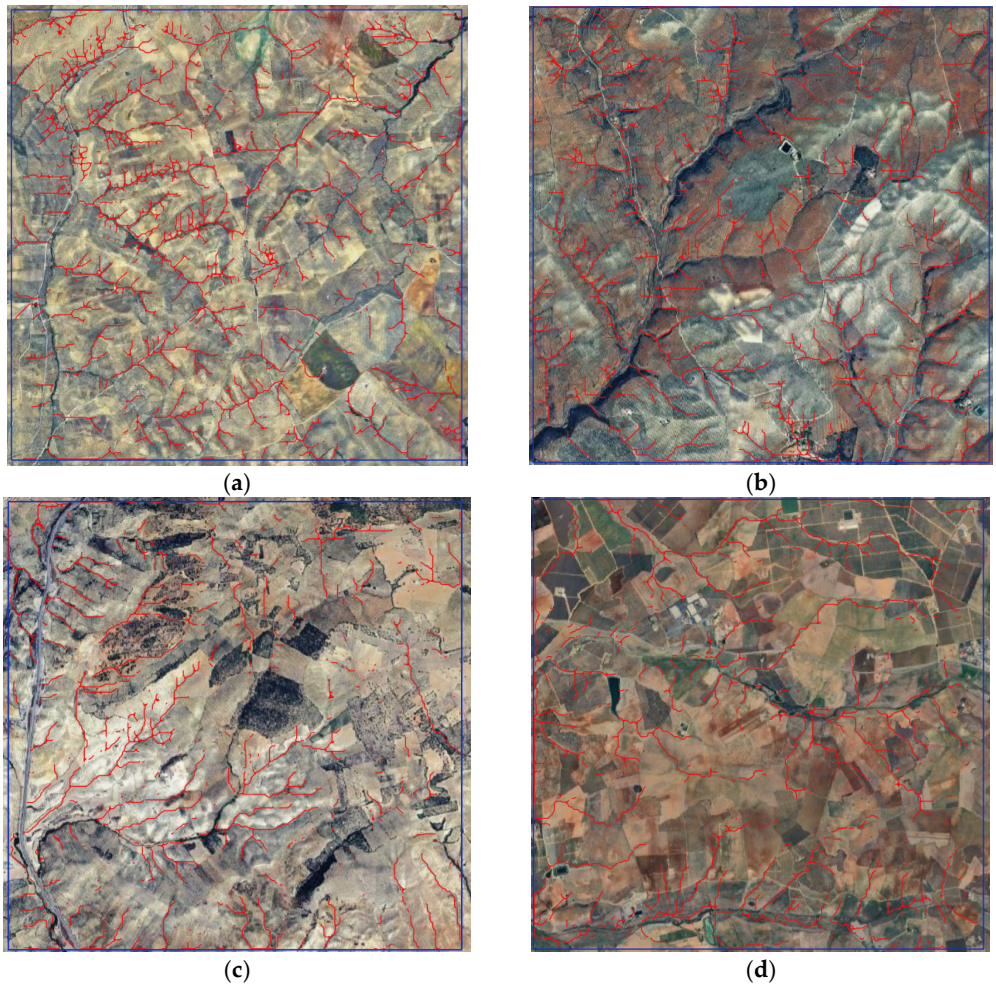

Figure 5. Examples of mapped gully network within four 25 km^2 study grid cells representing different landscape units: (**a**) Countryside hills; (**b**) Countryside foothills; (**c**) Mid-mountains; and (**d**) Valley plains.

4. Discussion

The study was based on the hypothesis that ML techniques could enhance the detection and spatial characterisation of gully erosion at a regional scale, overcoming the limitations of traditional approaches based exclusively on geomorphological thresholds or local-scale analyses [12,16,19–23,38]. In addition, it was hypothesised that incorporating variables derived from the GHI index [14,25], together with a revised formulation of this index, would provide key hydrological and topographic information and thereby improving model predictive performance.

To test these hypotheses, the performance of several classification algorithms was systematically evaluated, and their predictive behaviour was analysed in combination with a comprehensive set of geo-environmental predictors. The results support these hypotheses, revealing clear differences in model performance and in the relative contribution of the predictor variables. These aspects are examined in detail in the following sections.

4.1. Model Performance and Algorithm Comparison

Among the evaluated models, RF consistently outperformed the others, achieving the highest values for F1-score (0.8347), accuracy (0.8259), recall (0.8549), and AUC (0.9135). This indicates a well-balanced performance in terms of both predictive capability and effective detection of gully-affected areas. These results are consistent with numerous previous studies on gully erosion susceptibility mapping, in which RF has repeatedly

demonstrated superior performance compared to alternative algorithms. For instance, ref. [79], in a study conducted in eastern Iran, identified RF as the most accurate model for gully prediction, reaching an AUC of 0.96 and outperforming both single-tree approaches and probabilistic methods. In a similar vein, ref. [79] reported higher AUC, accuracy, and recall values for RF compared to regression-based and simple tree models, attributing this behaviour to its ability to capture non-linear relationships and reduce variance through tree ensembling. Furthermore, recent research has highlighted the efficacy of combining ML and hybrid approaches, such as FuzzyAHP–ML frameworks, in which RF continues to play a central role in the spatial identification of gully-susceptible areas [52].

The results obtained in this study are also consistent with regional-scale comparative research, such as that of [28], who evaluated different ML algorithms for gully erosion susceptibility mapping and reported high performance for RF (AUC = 0.933). In this context, the AUC value obtained for RF in the present study (0.9135) falls within the range commonly reported in the literature, reinforcing the robustness of the model even when applied to a broad and heterogeneous regional extent, such as the diverse landscape units analysed within the Guadalquivir Basin. Consequently, this model provides a reliable framework for the automated and spatially consistent mapping of gully network across Mediterranean olive-growing landscapes.

The robustness of the RF is attributed to its ability to address the limitations of individual DT by ensembling multiple predictors. As outlined by [66], RF employs bootstrap or bagging aggregation techniques to generate trees that differ from one another, thereby introducing randomness and significantly enhancing predictive performance [73]. Furthermore, the random selection of a subset of variables at each node reduces the risk of overfitting and enables robust modelling of complex, non-linear relationships. This process also provides estimates of variable importance [80]. Similar strengths have been reported in other studies addressing erosion and environmental processes, where RF has outperformed SVM in terms of predictive stability and consistency [81,82].

Nevertheless, the results indicate that SVM also achieved notable performance, with relatively high AUC (0.8092) and accuracy (0.7266) values, although these were consistently lower than those obtained by RF. This behaviour is consistent with the findings of [39], who reported that SVM can provide an effective balance between predictive accuracy and computational efficiency when applied to moderate-sized, well-refined predictor sets, as in the present study, which retained 17 variables after excluding SAVI and Kns due to VIF values exceeding 10. However, the lower recall of SVM compared to RF indicates a greater tendency to under-detect gully-affected areas, making it less appropriate when the primary objective is the exhaustive identification of the erosive network.

Conversely, less complex models, such as LG and DT, demonstrated lower overall performance, particularly in terms of recall. This suggests a reduced ability to accurately identify areas affected by gullies. This behaviour is likely related to the limited capacity of parametric models and single-tree approaches to represent complex non-linear relationships and multiple interactions among geo-environmental variables, as previously reported in geomorphological susceptibility studies [79,81]. In this context, the results further support the existing evidence that ensemble-based ML algorithms offer a clear advantage over traditional approaches when applied to large and heterogeneous geo-environmental datasets. This advantage is further evidenced by the False Classification Rate (FCR), which quantifies the operational risk for stakeholders by identifying the proportion of misclassifications among positive instances [76]. In our study, the RF model achieved a low FCR of 0.163, a result highly comparable to cutting-edge deep learning architectures like YOLOv10 (FCR = 0.152), which are noted for their high domain robustness in complex agricultural environments [76]. This low failure rate contrasts sharply with the LR model,

which exhibited a much higher FCR of 0.291. Such a high rate of failure—where nearly one in three identified gullies is an error—highlights why simpler parametric models are far too risky for actual remediation planning in landscapes where agricultural land leveling frequently masks or mimics topographic signatures. In contrast, the RF model's low FCR is a testament to its reliability for soil conservation planners, achieving an 83.7% operational success rate even in the noise-heavy Mediterranean olive groves.

4.2. Influence of Predictor Variables and the Role of the GHI Index

In this study, the highest model performance was achieved using the final set of 17 selected predictor variables. This indicates that RF benefits from a comprehensive representation of the hydrotopographic, climatic, edaphic, and surface cover factors controlling gully formation at the regional scale. Indeed, several RF-based gully susceptibility studies have relied on predictor sets of comparable size. For instance, ref. [83] used 11 variables, ref. [84] employed 12 variables, and ref. [85] considered 14 variables. In these studies, RF achieved AUC values ranging between 0.88 and 0.96, which are comparable to the accuracy obtained in the present study (AUC > 0.90). This reinforces both the suitability of the selected number of predictors and the robustness of the proposed model.

The Pearson correlation matrix (Figure 3) provides additional insight into the relationships among the selected predictors and helps contextualize their joint behaviour. As anticipated, the clay and sand contents exhibited a discernible negative correlation, reflecting the inherent trade-off between these texture fractions. Furthermore, the Curve Number (CN) generally increases with higher clay content, aligning with the lower permeability and higher runoff potential typically associated with finer-textured soils.

With regard to hydrotopographic controls, the two GHI formulations demonstrate a comparatively stronger association with flow accumulation than with their other input components. This suggests that the spatial pattern captured by the index is largely aligned with runoff concentration pathways. This behaviour may also be influenced by the heterogeneous spatial resolution of the predictors (e.g., flow-related variables versus coarser precipitation inputs). This can result in the dominance of variables that better preserve fine-scale spatial gradients within the modelling grid. In addition, a moderate positive correlation was observed between GHI and TWI (r = 0.35). This interaction is physically consistent, as both indices are driven by upslope contributing area (A). TWI is a method of measuring soil saturation, balancing A with the local slope to determine the propensity. By contrast, the GHI index focuses on the erosive energy of concentrated flow. The statistical correlation between these variables indicates that regions exhibiting high subsurface saturation potential frequently coincide with areas of significant surface runoff energy. Collectively, these factors delineate the most critical hotspots for gully incision.

In the context of surface-cover descriptors, vegetation indices (NDVI and EVI) demonstrate an inverse correlation with BSI, aligning with the differential signals captured by greenness versus bare soil. Finally, RDN shows a slightly higher association with the GHI index than Pmax, although the difference is modest. Despite these associations, the calculated Variance Inflation Factor (VIF) and Tolerance (TOL) values remained within acceptable thresholds. However, further exploration of dimensionality reduction is recommended for future studies.

A key finding of this study is the high predictive capacity of the GHI index, which emerges as one of primary determinants in the RF model. When both formulations of the index are considered jointly, GHI accounts for nearly 30% of the total model importance, thereby validating the objective of refining the representation of gully activity through machine-learning approaches. It is interesting to note that the formulation based on RDN shows a higher relative importance (14.63%) compared to the version based on Pmax (14.00%). Although this difference is subtle, the result is consistent with the findings of [12],

who showed that TT variability in Mediterranean olive groves is more closely related to precipitation indices that reflect the average intensity of rainy days than to isolated extreme events, concluding that the increases in gully density, which doubled its density, were attributed to highly erosive rainfall conditions during 2009–2011.

Furthermore, this slightly superior performance of the RDN-based GHI formulation compared to Pmax is physically plausible. While Pmax represents an isolated daily extreme, RDN is more representative of sustained rainfall-day intensity regimes that contribute to antecedent wetness conditions and runoff response. This is consistent with hydrological evidence showing that runoff response times in deep soil-mantled landscapes are strongly influenced by antecedent soil moisture and vadose-zone dynamics, and that runoff generation can be closely linked to subsurface flow convergence near channel heads [86]. In addition, global analyses identified RDN as a robust proxy of daily rainfall intensity and one of the rainfall metrics most strongly associated with spatial variability in gully head retreat, in combination with processes such as tension crack development and mass failure [49]. Taken together, these findings support the use of RDN as a rainfall descriptor that better captures the persistence of erosive conditions than a single-event maximum, which may explain its slightly improved performance in the present model.

Although the GHI was originally developed to identify initiation thresholds at gully heads—achieving an AUC of 0.93 [14]—its strong performance in this regional model is particularly revealing. The fact that it excels even when predicting points distributed along the entire gully network, and not only at initiation zones, suggests that the physical processes governing initial incision remain the dominant factors defining the morphology and persistence of the entire gully network.

It is also important to highlight that the GHI index was originally developed and validated in a semi-arid Ethiopian context [25], characterised by markedly different climatic, geomorphological, and land-use conditions compared to Mediterranean olive landscapes. The fact that the index demonstrated strong predictive performance both in that African semi-arid environment and in Mediterranean agricultural systems reinforces its process-based robustness. This cross-context consistency suggests that the underlying physical mechanism—the balance between runoff-induced shear stress and soil resistance—remains valid across contrasting environmental settings.

Beyond the GHI index, flow accumulation emerges as the most influential predictor, accounting for 17.33% of the total importance (Figure 4). This predominance of hydrological factors is in agreement with the findings of [39], who argue that the intensification of stream-flow power in areas with high hydrological connectivity constitutes the primary driver of gully incision. Similarly, ref. [87] reported that the intensity of gully head erosion largely depends on runoff volume and on variables reflecting flow concentration, such as drainage density, proximity to channels, and the Stream Power Index (SPI). This high relative importance of flow accumulation is particularly relevant for the structural consistency of the generated network. Although a DEM-based flow-routing procedure (e.g., D8) was not explicitly used to trace lines during the final vectorisation stage, the fact that the machine-learning classification was so strongly guided by flow accumulation ensures that the resulting raster inherently reflects the underlying hydrological skeleton of the landscape.

In the same vein, the TWI, which contributes 9.44% to the model, is consistent with the observations of [39], who found that more than 70% of gullies were located in areas with TWI values ranging between 6.13 and 7.53. This indicates a high propensity for soil saturation that substantially reduces soil resistance. In this context, these authors also identified TWI as one of the most influential predictors, with a relative importance close to 25%, reinforcing its key role as an indicator of hydrological accumulation and topographic control on incision processes. Furthermore, ref. [88] research demonstrated that excluding

TWI from the model results in a reduction in predictive performance ranging from 21% to 32%, depending on the algorithm used. This indicates that, although not the dominant factor, TWI plays a significant and non-negligible role in gully erosion susceptibility.

The variable ranking obtained in this study indicates that hydrotopographic factors exert a greater explanatory influence than vegetation cover and soil properties. This predominance of topography and hydrology is consistent with the findings of [52], who identified variables such as elevation, distance to channels, and drainage density as the most influential predictors, while vegetation indices played a secondary role. In this sense, the review by [89] highlights that research by [55] identified drainage density, rainfall, and S as the most effective predictors; similarly, in the study by [69], land cover reached a secondary level of importance relative to drainage density.

Nevertheless, recent research by [53] has demonstrated that NDVI plays a pivotal role in mitigating soil loss by representing the protective capacity of vegetation cover. However, its relative contribution can be overshadowed by topographic and hydrological controls in environments characterized by pronounced terrain gradients. This is consistent with the findings of the present study in Mediterranean olive groves, where vegetation indices exhibit comparatively low importance (NDVI: 3.87%; EVI: 3.32%). Similarly, the low contribution of soil properties observed in this study—such as clay content and silt content (3.26%)—contrasts with cases where soil type emerged as the dominant factor [88] or where clay content played a decisive role [90]. Likewise, the low standalone importance of the Curve Number (CN) is consistent with its limited spatial variability in the olive-dominated study region [14], while its effect becomes more informative when combined within the composite GHI formulations together with rainfall forcing and hydrotopographic controls.

The contrast between the high predictive power of hydrotopographic factors and the secondary role of vegetation indices reflects the hierarchy of processes in these landscapes. However, the findings of the Pearson analysis (Table 5) demonstrate a negative correlation between vegetation indices (NDVI and EVI) and gully occurrence, thus confirming the role of surface cover in mitigating erosion. In Mediterranean olive groves, vegetation cover is considered the primary ally in controlling sheet and rill erosion [51]. In contrast, the positive correlation of GHI is consistent with studies such as that of [14], which shows that higher GHI values represent exceeding critical runoff energy thresholds for soil detachment. Therefore, while relief and hydrology (GHI and flow accumulation) determine the physical potential for incision at a regional scale, maintaining adequate vegetation cover remains the most effective and viable management tool for farmers to mitigate gully expansion and stabilize existing networks.

Within the field of Gully Erosion Susceptibility Mapping (GESM), it is common for a variable identified as the most important predictor in one study to rank much lower in another. For instance, ref. [81] found S to exert the strongest influence on gully erosion, whereas ref. [84] reported it as the least important factor. As suggested by [38,91], such discrepancies may arise from differences in spatial context, uncertainties in variable quantification, or substantial variation in the effect of predictors across contrasting environments.

Despite this variability, there is broad consensus that primary geographic attributes (elevation, S, curvature), hydrological properties (precipitation), and anthropogenic factors (land use) rank among the most influential predictors affecting the quality of susceptibility models [81,84,92]. In the specific case of the olive-growing landscapes analysed here, terrain morphometry and flow concentration clearly prevail over intrinsic soil resistance or the instantaneous state of vegetation in shaping the architecture of the gully network.

Finally, the spatial resolution and availability of the input data are key factors for model scalability. While the use of very high spatial resolutions (1–2 m), such as those adopted by [93,94], has been shown to yield excellent predictive performance, their application

is typically limited to small catchments (<11 km^2) due to the high costs associated with data acquisition and processing. In contrast, refs. [69,81] have demonstrated that spatial resolutions in the range of 20–30 m can provide satisfactory results for gully detection at broader spatial scales. Consequently, the integration of 30 m elevation data resampled to 10 m effectively overcomes the limitations associated with ultra-high-resolution datasets in local-scale applications, while maintaining a robust and efficient capacity for detecting gully network across the Guadalquivir Basin. Furthermore, the CHIRPS and Copernicus DEM datasets, from which the model's most influential hydrotopographic variables were derived, are available at a global scale. Consequently, model scalability is not constrained by the need for local-scale data, ensuring the transferability of this approach to other regions.

4.3. Spatial Patterns of the Gully Network Across Landscapes

The results of this study confirm that the highest gully network densities are concentrated within countryside landscapes, specifically reaching 42.50 m/ha in the countryside hills and 40.10 m/ha in the countryside foothills. These figures are notably higher than those recorded in the mid-mountains (31.43 m/ha) and the valley plains (30.58 m/ha). This spatial distribution aligns with the findings of [11], which identify the olive-growing countryside landscapes of the Guadalquivir Basin as environments of extreme vulnerability. In such systems, gully erosion can represent the primary source of sediment, significantly exceeding inter-rill and rill erosion rates and acting as the main driver of soil degradation at the basin scale.

While the study by [11] reported a higher density of 53.3 m/ha for a specific countryside micro-catchment, this discrepancy is expected. Their research was conducted at a local scale (<20 km^2), allowing for an exhaustive characterization of the network influenced by site-specific dynamic. In contrast, the present regional-scale analysis provides a representative average across diverse landscape units. Furthermore, this difference is justified by the post-processing protocol adopted in this study, in which infrastructures, roads, and permanent stream channels were systematically excluded, thereby ensuring that the mapped network corresponds exclusively to gully features. Additionally, the slightly lower density values in our regional assessment may reflect the influence of gully infilling due to agricultural land levelling, a common practice in Mediterranean olive groves that masks ephemeral segments and which is further detailed in the limitations section of this work.

In a broader Mediterranean context, reported gully density values remain scarce and are often not directly comparable due to differences in mapping scale, gully definition (ephemeral vs. persistent), and delineation procedures. Nevertheless, available benchmarks indicate lower density values than those obtained in our regional olive-growing landscapes. For example, ref. [95] reported an average ephemeral gully length of 1696 m yr^{-1} in an ≈80 ha monitored agricultural area in southern Italy, corresponding to 21 m ha^{-1} yr^{-1}, while [96] reported an average total gully length equivalent to 13.6 m ha^{-1} across sampled Mediterranean agricultural surfaces in Greece, including olive groves. These reference values provide an approximate range for Mediterranean agricultural settings and highlight the relevance of reporting gully network density in consistent units at regional scale.

Furthermore, the higher gully density observed in the countryside correlates with the high erosive activity described in previous studies for these areas [14]. In that research, by applying the GHI to gully heads across the four landscape units, a higher rate of new gullies was observed in the countryside compared to mid-mountain and valley plains, which exhibited a greater number of inactive gullies during the 2008–2019 period. This pattern is further supported by the gully head density analysis, where valley plains and mountain areas showed the lowest values at 1.08 and 0.64 heads km^{-2}, respectively, while countryside landscapes reached significantly higher densities of 3.16 heads km^{-2}. These findings are

consistent with the gully length densities reported in the present study, reinforcing the role of countryside areas as the most active erosion hotspots.

From a geomorphological perspective, these spatial contrasts can be interpreted in light of the intrinsic structural and hydrological characteristics of each landscape unit [33]. The countryside hills, which represent the most homogeneous and agriculturally specialised landscape, combine gentle but continuous slopes with clay-rich soils and extensive olive groves areas. This configuration promotes surface runoff concentration during high-intensity rainfall events, enhancing hydrotopographic connectivity and favouring the incision and lateral expansion of gullies. In contrast, the countryside foothills, despite exhibiting steeper slopes, are characterised by greater relief heterogeneity and land-use mosaic patterns and more stoniness, which may locally disrupt runoff continuity. The mid-mountain landscapes, with sandier soils and reduced water retention capacity, display a differentiated hydrological response, potentially limiting sustained concentrated flow despite their altimetric prominence. Finally, the valley plains, despite receiving higher annual precipitation, are characterised by gentler topographies and more balanced soil textures. These conditions reduce slope-driven shear stress, which partly explains their comparatively lower gully network densities. Therefore, the observed spatial distribution of the gully network reflects not only climatic forcing but also the structural organisation of relief, soil properties, and land-use configuration within each geomorphological unit [14].

4.4. Study Limitations

One of the main limitations of this study lies in the difficulty of capturing the complete gully network due to infilling processes induced by agricultural activities. As noted by [11,12], in Mediterranean olive-growing landscapes, land levelling practices aimed at facilitating machinery traffic frequently result in the artificial infilling of gully segments, thereby visually masking ephemeral or partially active gullies. This behaviour is embedded within a non-linear dynamic of gully growth and stabilisation, as described by [97], in which phases of rapid incision may alternate with periods of sediment infilling and apparent morphological stability.

In addition, the variability in gully growth and retreat rates, extensively documented by [49], reflects strong interannual variability driven by short-lived, high-intensity rainfall events. Consequently, analyses based on discrete temporal observations may fail to fully capture the magnitude and dynamics of erosive processes, particularly following extreme precipitation events. To partially address this limitation, the present study incorporates integrated pluviometric information through the calculation of maximum precipitation and the RDN using three-year moving windows for each pixel, thus providing a partial representation of the cumulative effects of extreme events between observation periods.

Nevertheless, because the model relies on photointerpretation of specific temporal images, the actual gully density may be underestimated, as anthropogenic land management practices can obscure the development and expansion of the gully network between observation dates. This agricultural "cleaning" of gullies introduces an inherent uncertainty in regional-scale quantification that is difficult to resolve without continuous field monitoring. Accordingly, the gully network generated in this study primarily represents the most persistent and morphologically developed segments that have resisted repeated land management features. Despite the inherent difficulty of detecting gullies in areas subjected to infilling, the RF model demonstrates high reliability in overcoming the topographic noise created by agricultural smoothing. This is reflected in the low FCR of 0.163, which, following the framework of [76], effectively summarizes the operational impact of these modifications. The FCR captures the balance between missing active gullies (False Negatives) and incorrectly flagging subtle depressions or recently infilled segments (False

Positives). The fact that the model maintains an 83.7% reliability rate confirms its ability to discern real erosive areas even when land leveling has sought to mask them, making it a robust tool for mapping in managed Mediterranean landscapes.

Furthermore, while the masking procedure applied to roads and the official hydrographic network is necessary to minimise false positives associated with linear infrastructures and permanent channels, it may inadvertently exclude real gully segments located in close proximity to these features. This is an additional source of uncertainty inherent to regional-scale automated mapping approaches, particularly in highly managed agricultural landscapes where anthropogenic and erosive linear features may spatially overlap.

Please note that there is an additional limitation relating to the spatial resolution of the precipitation data. CHIRPS rainfall products, initially available at 5 km resolution, were resampled to 10 m to ensure spatial consistency with the remaining predictors within the machine-learning framework. Whilst this procedure permits pixel-level integration of variables, it does not introduce additional fine-scale climatic information and may smooth local rainfall variability. Consequently, highly localised convective precipitation patterns that can trigger gully initiation at very small spatial scales may not be fully captured. Although the use of CHIRPS ensures methodological consistency and facilitates potential model scalability to other regions, this resolution mismatch represents an inherent source of uncertainty in regional-scale applications.

The model has been designed to be scalable and is based on widely available datasets (e.g., CHIRPS, Copernicus DEM, Sentinel-2). However, its formal validation in other olive-growing regions or Mediterranean environments has not yet been conducted. Therefore, while the methodological framework ensures structural transferability, further interregional testing will be required before confirming its external regional applicability. Furthermore, the model's conceptual domain of applicability is primarily linked to gully incision processes driven by concentrated surface runoff. Consequently, its transferability may be limited in environments where channel initiation is not predominantly controlled by overland flow dynamics. It is recommended that future research assess the model's performance under a range of climatic, geomorphological and land-management conditions. This will provide an indication of the model's robustness beyond the Guadalquivir Basin.

Finally, the accuracy of the model is constrained by limitations in the spatial resolution and inherent heterogeneity of some input datasets. In this regional-scale model, edaphic properties such as clay, silt, and coarse fragment content were found to be relatively unimportant. This behaviour can largely be attributed to the insufficient spatial resolution of the available soil maps. In this study, most soil properties were derived from products with a spatial resolution of 100 m, while coarse fragment content was obtained from more generalized datasets at 500 m resolution (Table 1). This indicates a mismatch in the spatial scale of the available soil datasets and the physical process under study. While these products provide robust regional characterisation, gully initiation and development are significantly influenced by fine-scale soil heterogeneity. At pixel sizes ranging from 100 to 500 m, subpixel variability in soil structure, stoniness, and surface sealing is statistically smoothed. This can potentially mask the influence of soil texture on runoff generation and erodibility. Consequently, it may reduce its apparent predictive power relative to hydrotopographic indices that preserve spatial gradients more effectively at the modelling scale.

5. Conclusions

This study presents a robust methodological framework for the automated generation of gully networks in olive groves across the Guadalquivir Basin. This is achieved by integrating ML algorithms with hydrotopographic, climatic, edaphic factors and physically based indices like the GHI, yielding a mapped network totaling 8439.05 km. The results

demonstrate that the RF algorithm outperformed SVM, DT, and LR models in terms of accuracy and robustness, as evidenced by an AUC of 0.9135 and an F1-score of 0.8347. These metrics indicate a high-level predictive capability and an optimal balance between precision and recall.

The robust performance of RF further highlights the suitability of non-linear modelling approaches in capturing the complexity of erosion processes at extensive spatial scales, enabling a shift from local photointerpretation-based inventories toward scalable and dynamic predictive mapping frameworks.

A key finding of this research is the significance of the GHI index as a fundamental predictor of the gully network. The inclusion of the two formulations accounted for almost 30% of the total model importance, with the RDN-based GHI demonstrating slightly higher explanatory power (14.63%) than the formulation based on maximum daily precipitation. In conjunction with flow accumulation, which emerged as the most influential individual predictor (17.33%), the GHI index constitutes a pivotal component for strengthening model robustness across Mediterranean agricultural landscapes. These results indicate that gully network persistence is more closely linked to rainfall intensity during wet days than to isolated extreme events. Furthermore, the analysis confirms the dominant role of hydrotopographic controls in mapping the gully network, substantially outweighing the contribution of edaphic and vegetation-related variables.

From a geographical perspective, the generated gully network reveals a markedly heterogeneous spatial distribution of soil degradation. The countryside landscapes (hills and foothills) are evidently the most affected areas, exhibiting the highest gully densities, with values reaching up to 42.50 m ha^{-1}. These figures are significantly higher than those observed in mid-mountain landscapes (31.43 m ha^{-1}) and valley plains (30.58 m ha^{-1}), positioning these countryside areas as erosion hotspots that demand priority management and intervention.

Furthermore, the developed model—built on accessible datasets and spatially harmonised to a 10 m resolution—constitutes an operational and transferable tool for land-use planning. While previous research has frequently been limited to local studies or susceptibility maps, this methodology represents a significant advancement by generating a continuous, regional-scale gully network. By precisely identifying areas of concentrated erosion and high hydrological connectivity, this comprehensive cartographic framework highlights the true extent of degradation in Mediterranean countryside olive groves. Ultimately, this baseline data provides a critical tool for targeted prevention and restoration, supporting the long-term sustainability of the olive sector by addressing the urgent challenge of soil loss.

Author Contributions: Conceptualization, P.G.-G., A.P.-A. and J.J.-T.; methodology, P.G.-G., A.P.-A. and J.J.-T.; software, P.G.-G. and J.J.-T.; validation, P.G.-G. and J.J.-T.; formal analysis, P.G.-G. and J.J.-T.; investigation, P.G.-G.; resources, P.G.-G. and J.J.-T.; data curation, P.G.-G. and J.J.-T.; writing—original draft preparation, P.G.-G. and A.P.-A.; writing—review and editing, P.G.-G., A.P.-A. and F.-J.M.-C.; visualization, F.-J.M.-C.; supervision, A.P.-A.; project administration, A.P.-A.; funding acquisition, A.P.-A. All authors have read and agreed to the published version of the manuscript.

Funding: This research has been developed within the framework of the CARCAVA project (ProyExcel_00700; 180.000 €) "Climatic and Agronomic Influence on the Formation and Evolution of the Gully Network in the Andalusian Countryside," funded by the Ministry of University, Research, and Innovation of Government of Andalucia, within the scope of the Andalusian Plan for Research, Development and Innovation (PAIDI 2020).

Data Availability Statement: The original contributions presented in this study are included in the article. Further inquiries can be directed to the corresponding author.

Acknowledgments: Also, this research is part of the ENIA International Chair in Agriculture, University of Córdoba (TSI-100921-2023-3), funded by the Secretary of State for Digitalization and Artificial Intelligence and by the European Union-Next Generation EU. Recovery, Transformation and Resilience Plan.

Conflicts of Interest: Author Juan Julca Torres was employed by the company REALIMA INGENIERÍA AMBIENTAL. The remaining authors declare that the research was conducted in the absence of any commercial or financial relationships that could be construed as a potential conflict of interest.

Abbreviations

The following abbreviations are used in this manuscript:

ML	Machine Learning
RF	Random Forest
SVM	Support Vector Machine
LR	Logistic Regression
DT	Decision Tree
FCR	False Classification Rate
GHI	Gully Head Initiation
RDN	Rainy Day Normal
DEM	Digital Elevation Model
SSI	Shear Stress index
CSI	Critical Shear Stress index
TT	Topographic Threshold
CHIRPS	Climate Hazards Groups Infrared Precipitation with Station data
ESDAC	European Soil Data Center
REDIAM	Andalusian Environmental Information Network
ESA	European Space Agency
SIOSE	Spanish Land Use Information System
PNOA	National Plan for Aerial Orthophotography
VIF	Variance Inflation Factor
S	Slope
A	Drainage area
BSI	Bare Soil Index
NDVI	Normalized Difference Vegetation Index
SAVI	Soil-Adjusted Vegetation Index
EVI	Enhanced Vegetation Index
Pmax	Maximum daily precipitation
TWI	Topographic Wetness Index
Kns	Normalized Steepness Index
AUC	Area Under the Curve
RUSLE	Revised Universal Soil Loss Equation

References

1. Panagos, P.; Broothaerts, N.; Ballabio, C.; Orgiazzi, A.; De Rosa, D.; Borrelli, P.; Jones, A. How the EU soil observatory is providing solid science for healthy soils. *Eur. J. Soil Sci.* **2024**, *75*, e13507. [CrossRef]
2. Borrelli, P.; Panagos, P.; Alewell, C.; Ballabio, C.; De Oliveira Fagundes, H.; Haregeweyn, N.; Lugato, E.; Maerker, M.; Poesen, J.; Vanmaercke, M.; et al. Policy implications of multiple concurrent soil erosion processes in European farmland. *Nat. Sustain.* **2022**, *6*, 103–112. [CrossRef]
3. Panagos, P.; Montanarella, L.; Barbero, M.; Schneegans, A.; Aguglia, L.; Jones, A. Soil priorities in the European Union. *Geodermal Reg.* **2022**, *29*, e00510. [CrossRef]
4. EU Nature Restoration Act. Available online: https://ec.europa.eu (accessed on 20 January 2024).
5. Poesen, J.; Nachtergaele, J.; Verstraeten, G.; Valentin, C. Gully erosion and environmental change: Importance and research needs. *Catena* **2003**, *50*, 91–133. [CrossRef]

6. Valentin, C.; Poesen, J.; Li, Y. Gully erosion: Impacts, factors and control. *Catena* **2005**, *63*, 132–153. [CrossRef]
7. Kuhn, C.E.S.; Reis, F.A.G.V.; Zarfl, C.; Grathwohl, P. Ravines and gullies, a review about impact valuation. *Nat. Hazards* **2023**, *117*, 597–624. [CrossRef]
8. Poesen, J.; Vandekerckhove, L.; Nachtergaele, J.; Wijdenes, D.O.; Verstraeten, G.; Van Wesemael, B. Gully erosion in dryland environments. In *Dryland Rivers: Hydrology and Geomorphology of Semi-Arid Channels*; Bull, L.J., Kirkby, M.J., Eds.; John Wiley & Sons: Chichester, UK, 2002; pp. 229–262.
9. Frankl, A.; Poesen, J.; Haile, M.; Deckers, J.; Nyssen, J. Quantifying long-term changes in gully networks and volumes in dryland environments: The case of northern Ethiopia. *Geomorphology* **2013**, *201*, 254–263. [CrossRef]
10. Dewitte, O.; Daoudi, M.; Bosco, C.; Van Den Eeckhaut, M. Predicting the susceptibility to gully initiation in data-poor regions. *Geomorphology* **2015**, *228*, 101–115. [CrossRef]
11. Hayas, A.; Vanwalleghem, T.; Laguna, A.; Peña, A.; Giráldez, J.V. Reconstructing long-term gully dynamics in Mediterranean agricultural areas. *Hydrol. Earth Syst. Sci.* **2017**, *21*, 235–249. [CrossRef]
12. Hayas, A.; Poesen, J.; Vanwalleghem, T. Rainfall and vegetation effects on temporal variation of topographic thresholds for gully initiation in Mediterranean cropland and olive groves. *Land Degrad. Dev.* **2017**, *28*, 2540–2552. [CrossRef]
13. Castillo, C. Metodología de Medida de la Erosión por Cárcavas y Modelado de su Control Mediante Diques de Retención. Ph.D. Thesis, University of Córdoba, Córdoba, Spain, 2012.
14. González, P.; Peña, A.; De Geeter, S.; Vanmaercke, M.; Poesen, J.; Vanwalleghem, T. What drives gullies in Spain's olive landscapes? A regional analysis of gully activity. *Catena* **2026**, *263*, 109699. [CrossRef]
15. Castillo, C.; Gómez, J.A. A century of gully erosion research: Urgency, complexity and study approaches. *Earth-Sci. Rev.* **2016**, *160*, 300–319. [CrossRef]
16. Vanmaercke, M.; Panagos, P.; Vanwalleghem, T.; Hayas, A.; Foerster, S.; Borrelli, P.; Rossi, M.; Torri, D.; Casali, J.; Borselli, L.; et al. Measuring, modelling and managing gully erosion at large scales: A state of the art. *Earth-Sci. Rev.* **2021**, *218*, 103637. [CrossRef]
17. Tan, Z.; Leung, L.R.; Li, H.; Cohen, S. Representing global soil erosion and sediment flux in Earth system models. *J. Adv. Model. Earth Syst.* **2021**, *14*, e2021MS002756. [CrossRef]
18. Panagos, P.; Borrelli, P.; Poesen, J.; Ballabio, C.; Lugato, E.; Meusburger, K.; Montanarella, L.; Alewell, C. The new assessment of soil loss by water erosion in Europe. *Environ. Sci. Policy* **2015**, *54*, 438–447. [CrossRef]
19. Vandaele, K.; Poesen, J.; Govers, G.; Van Wesemael, B. Geomorphic threshold conditions for ephemeral gully incision. *Geomorphology* **1996**, *16*, 161–173. [CrossRef]
20. Vandekerckhove, L.; Poesen, J.; Wijdenes, D.O.; De Figueiredo, T. Topographical thresholds for ephemeral gully initiation in intensively cultivated areas of the Mediterranean. *Catena* **1998**, *33*, 271–292. [CrossRef]
21. Vandekerckhove, L.; Poesen, J.; Oostwoud-Wijdenes, D.; Nachtergaele, J.; Kosmas, C.; Roxo, M.J.; de Figueiredo, T. Thresholds for gully initiation and sedimentation in Mediterranean Europe. *Earth Surf. Process. Landf.* **2000**, *25*, 1201–1220. [CrossRef]
22. Imaizumi, F.; Hattanji, T.; Hayakawa, Y.S. Channel initiation by surface and subsurface flows in a steep catchment of the Akaishi Mountains, Japan. *Geomorphology* **2010**, *115*, 32–42. [CrossRef]
23. Torri, D.; Poesen, J. A review of topographic threshold conditions for gully head development in different environments. *Earth-Sci. Rev.* **2014**, *130*, 73–85. [CrossRef]
24. Rossi, M. Modeling of Landslide Phenomena and Erosion Processes Triggered by Meteo-Climatic Factors. Ph.D. Thesis, Università Degli Studi Di Perugia, Perugia, Italy, 2014.
25. De Geeter, S.; Setargie, T.A.; Haregeweyn, N.; Verstraeten, G.; Poesen, J.; Tsunekawa, A.; Vanmaercke, M. Advancing gully initiation modelling by means of a Curve Number (CN) method: A way forward? *Earth Surf. Process. Landf.* **2025**, *50*, e70145. [CrossRef]
26. Knapen, A.; Poesen, J.; Govers, G.; Gyssels, G.; Nachtergaele, J. Resistance of soils to concentrated flow erosion: A review. *Earth-Sci. Rev.* **2007**, *80*, 75–109. [CrossRef]
27. Vannoppen, W.; Vanmaercke, M.; De Baets, S.; Poesen, J. A review of the mechanical effects of plant roots on concentrated flow erosion rates. *Earth-Sci. Rev.* **2015**, *150*, 666–678. [CrossRef]
28. Arabameri, A.; Chandra Pal, S.; Costache, R.; Saha, A.; Rezaie, F.; Seyed Danesh, A.; Pradhan, B.; Lee, S.; Hoang, N.-D. Prediction of gully erosion susceptibility mapping using novel ensemble machine learning algorithms. *Geomat. Nat. Hazards Risk* **2021**, *12*, 469–498. [CrossRef]
29. Saha, S.; Roy, J.; Arabameri, A.; Blaschke, T.; Tien Bui, D. Machine Learning-Based Gully Erosion Susceptibility Mapping: A Case Study of Eastern India. *Sensors* **2020**, *20*, 1313. [CrossRef] [PubMed]
30. Borrelli, P.; Matthews, F.; Alewell, C.; Kaffas, K.; Poesen, J.; Saggau, P.; Prăvălie, R.; Vanmaercke, M.; Panagos, P. A hybrid in situ and on-screen survey to monitor gully erosion across the European Union. *Sci. Data* **2025**, *12*, 755. [CrossRef]
31. Peel, M.C.; Finlayson, B.L.; McMahon, T.A. Updated world map of the Köppen-Geiger climate classification. *Hydrol. Earth Syst. Sci.* **2007**, *11*, 1633–1644. [CrossRef]

32. Encuesta Sobre Superficies y Rendimientos Cultivos (ESYRCE). Available online: https://www.mapa.gob.es/es/estadistica/temas/estadisticas-agrarias/agricultura/esyrce/ (accessed on 12 January 2024).
33. Moreira Madueño, J.M.; Cáceres Clavero, F.; Giménez de Azcárate Fernández, F.; Olmedo Granados, F.; Briones Alcañiz, M.; Aparicio Martínez, J.; Ghislanzoni, M.; Torres García, M. *Paisajes de Andalucía; Consejería de Agricultura, Ganadería, Pesca y Desarrollo Sostenible*; Junta de Andalucía: Sevilla, Espana, 2018; pp. 1–106.
34. O'Callaghan, J.F.; Mark, D.M. The extraction of drainage networks from digital elevation data. *Comput. Vis. Graph. Image Process.* **1984**, *28*, 323–344. [CrossRef]
35. Tarboton, D.G. A new method for the determination of flow directions and upslope areas in grid digital elevation models. *Water Resour. Res.* **1997**, *33*, 309–319. [CrossRef]
36. Quinn, P.; Beven, K.; Chevallier, P.; Planchon, O. The prediction of hillslope flow paths for distributed hydrological modelling using digital terrain models. *Hydrol. Process.* **1991**, *5*, 59–79. [CrossRef]
37. Jones, R. Algorithms for using a DEM for mapping catchment areas of stream sediment samples. *Comput. Geosci.* **2002**, *28*, 1051–1060. [CrossRef]
38. Gutiérrez, Á.G.; Schnabel, S.; Contador, F.L. Gully erosion, land use and topographical thresholds during the last 60 years in a small rangeland catchment in SW Spain. *Land Degrad. Dev.* **2009**, *20*, 535–550. [CrossRef]
39. Phinzi, K.; Szabó, S. Predictive machine learning for gully susceptibility modeling with geo-environmental covariates: Main drivers, model performance, and computational efficiency. *Nat. Hazards* **2024**, *120*, 7211–7244. [CrossRef]
40. Beven, K.J.; Kirkby, M.J. A physically based, variable contributing area model of basin hydrology. *Hydrol. Sci. J.* **1979**, *24*, 43–69. [CrossRef]
41. Sörensen, R.; Zinko, U.; Seibert, J. On the calculation of the topographic wetness index: Evaluation of different methods based on field observations. *Hydrol. Earth Syst. Sci.* **2006**, *10*, 101–112. [CrossRef]
42. Flint, J.J. Stream gradient as a function of order, magnitude, and discharge. *Water Resour. Res.* **1974**, *10*, 969–973. [CrossRef]
43. Willett, S.D.; Hovius, N.; Brandon, M.T.; Fisher, D.M. (Eds.) Introduction. In *Tectonics, Climate and Landscape Evolution*; Geological Society of America (GSA): Boulder, CO, USA, 2006; Volume 398.
44. Montgomery, D.R.; Dietrich, W.E. Landscape dissection and drainage area-slope thresholds. In *Process Models and Theoretical Geomorphology*; John Wiley & Sons: Hoboken, NJ, USA, 1994; pp. 221–246.
45. Nearing, M.A.; Norton, L.D.; Bulgakov, D.A.; Larionov, G.A.; West, L.T.; Dontsova, K.M. Hydraulics and erosion in eroding rills. *Water Resour. Res.* **1997**, *33*, 865–876. [CrossRef]
46. Nachtergaele, J.; Poesen, J.; Sidorchuk, A.; Torri, D. Prediction of concentrated flow width in ephemeral gully channels. *Hydrol. Process.* **2002**, *16*, 1935–1953. [CrossRef]
47. Hawkins, R.H.; Ward, T.J.; Woodward, D.E.; Van Mullem, J.A. *Curve Number Hydrology: State of the Practice*; ASCE/EWRI: Reston, VA, USA, 2009.
48. Nachtergaele, J.; Poesen, J.; Steegen, A.; Takken, I.; Beuselinck, L.; Vandekerckhove, L.; Govers, G. The value of a physically based model versus an empirical approach in the prediction of ephemeral gully erosion for loess-derived soils. *Geomorphology* **2001**, *40*, 237–252. [CrossRef]
49. Vanmaercke, M.; Poesen, J.; Van Mele, B.; Demuzere, M.; Bruynseels, A.; Golosov, V.; Bezerra, J.F.R.; Bolysov, S.; Dvinskih, A.; Frankl, A.; et al. How fast do gully headcuts retreat? *Earth-Sci. Rev.* **2016**, *154*, 336–355. [CrossRef]
50. Wischmeier, W.H.; Smith, D.D. *Predicting Rainfall Erosion Losses—A Guide to Conservation Planning*; USDA Agriculture Handbook No. 537; U.S. Government Printing Office: Washington, DC, USA, 1978.
51. Guzmán Álvarez, J.R. The forests and rural landscapes of Andalusia. In *Agroforestry Systems as a Technique for Sustainable Land Management*, 1st ed.; Mosquera Losada, M.R., Rigueiro Rodríguez, A., Fernández Lorenzo, J.L., Eds.; Unicopia: Lugo, Spain, 2009; pp. 95–104.
52. Singha, C.; Swain, K.C.; Pradhan, B.; Alamri, A. Integration of FuzzyAHP and machine learning algorithms for climate-driven gully erosion susceptibility mapping: Predicting future trends in the eastern lateritic region, West Bengal, India. *Geosci. J.* **2024**, *28*, 981–1011. [CrossRef]
53. Uyar, N. Index-Driven Soil Loss Mapping Across Environmental Scenarios: Insights from a Remote Sensing Approach. *Sustainability* **2025**, *17*, 7913. [CrossRef]
54. Arabameri, A.; Rezaei, K.; Pourghasemi, H.R.; Lee, S.; Yamani, M. GIS-based gully erosion susceptibility mapping: A comparison among three data-driven models and AHP knowledge-based technique. *Environ. Earth Sci.* **2018**, *77*, 628. [CrossRef]
55. Arabameri, A.; Cerdà, A.; Pradhan, B.; Tiefenbacher, J.P.; Lombardo, L.; Bui, D.T. A methodological comparison of head-cut based gully erosion susceptibility models: Combined use of statistical and artificial intelligence. *Geomorphology* **2020**, *359*, 107136. [CrossRef]
56. Arabameri, A.; Saha, S.; Chen, W.; Roy, J.; Pradhan, B.; Bui, D.T. Flash flood susceptibility modelling using functional tree and hybrid ensemble techniques. *J. Hydrol.* **2020**, *587*, 125007. [CrossRef]

57. Du, G.; Zhang, Y.; Iqbal, J.; Yang, Z.; Yao, X. Landslide susceptibility mapping using an integrated model of information value method and logistic regression in the Bailongjiang watershed, Gansu Province, China. *J. Mt. Sci.* **2017**, *14*, 249–268. [CrossRef]
58. Bui, D.T.; Pradhan, B.; Lofman, O.; Revhaug, I.; Dick, O.B. Spatial prediction of landslide hazards in Hoa Binh province (Vietnam): A comparative assessment of the efficacy of evidential belief functions and fuzzy logic models. *Catena* **2012**, *96*, 28–40. [CrossRef]
59. Benesty, J.; Chen, J.; Huang, Y.; Cohen, I. *Noise Reduction in Speech Processing*; Springer: Berlin/Heidelberg, Germany, 2009.
60. Liakos, K.G.; Busato, P.; Moshou, D.; Pearson, S.; Bochtis, D. Machine learning in agriculture: A review. *Sensors* **2018**, *18*, 2674. [CrossRef]
61. Voyant, C.; Notton, G.; Kalogirou, S.; Nivet, M.L.; Paoli, C.; Motte, F.; Fouilloy, A. Machine learning methods for solar radiation forecasting: A review. *Renew. Energy* **2017**, *105*, 569–582. [CrossRef]
62. Chlingaryan, A.; Sukkarieh, S.; Whelan, B. Machine learning approaches for crop yield prediction and nitrogen status estimation in precision agriculture: A review. *Comput. Electron. Agric.* **2018**, *151*, 61–69. [CrossRef]
63. Pedregosa, F.; Varoquaux, G.; Gramfort, A.; Michel, V.; Thirion, B.; Grisel, O.; Blondel, M.; Prettenhofer, P.; Weiss, R.; Dubourg, V.; et al. Scikit-learn: Machine learning in Python. *J. Mach. Learn. Res.* **2011**, *12*, 2825–2830.
64. Phinzi, K.; Abriha, D.; Bertalan, L.; Holb, I.; Szabó, S. Machine Learning for Gully Feature Extraction Based on a Pan-Sharpened Multispectral Image: Multiclass vs. Binary Approach. *ISPRS Int. J. Geo-Inf.* **2020**, *9*, 252. [CrossRef]
65. Märker, M.; Pelacani, S.; Schröder, B. A functional entity approach to predict soil erosion processes in a small Plio-Pleistocene Mediterranean catchment in Northern Chianti, Italy. *Geomorphology* **2011**, *125*, 530–540. [CrossRef]
66. Breiman, L. Random Forests. *Mach. Learn.* **2001**, *45*, 5–32. [CrossRef]
67. Cortes, C.; Vapnik, V. Support-Vector Networks. *Mach. Learn.* **1995**, *20*, 273–297. [CrossRef]
68. Marjanović, M.; Kovačević, M.; Bajat, B.; Voženílek, V. Landslide susceptibility assessment using SVM machine learning algorithm. *Eng. Geol.* **2011**, *123*, 225–234. [CrossRef]
69. Akgün, A.; Türk, N. Mapping erosion susceptibility by a multivariate statistical method: A case study from the Ayvalık region, NW Turkey. *Comput. Geosci.* **2011**, *37*, 1515–1524. [CrossRef]
70. García Ojeda, J.G. Determinación de Algoritmos de Clasificación Óptimos Para la Evaluación de Riesgo Crediticio en el Caso de PyMES: Caso de Estudio: PyMES Que Operan en Plataformas P2P. Master's Thesis, Universidad Nacional de Cuyo, Mendoza, Argentina, 2023.
71. Quinlan, J.R. Induction of Decision Trees. *Mach. Learn.* **1986**, *1*, 81–106. [CrossRef]
72. Serra, A. Comparación de Algoritmos de Clasificación Supervisada. Master's Thesis, Escola Tècnica Superior d'Enginyeria Industrial de Barcelona, Barcelona, Spain, 2020.
73. Irizarry, R.A. *Introduction to Data Science: Data Analysis and Prediction Algorithms with R*; CRC Press: Boca Raton, FL, USA, 2019.
74. Kleinbaum, D.G.; Klein, M. Modeling Strategy Guidelines. In *Logistic Regression: A Self-Learning Text*, 3rd ed.; Springer: New York, NY, USA, 2010; pp. 161–189.
75. Hosmer, D.W.; Lemeshow, S. *Applied Logistic Regression*, 2nd ed.; John Wiley & Sons: New York, NY, USA, 2000; pp. 1–392.
76. Rana, S.; Hensel, O.; Nasirahmadi, A. From vineyard to vision: Multi-domain analysis and mitigation of grape cluster detection failures in complex viticultural environments. *Results Eng.* **2026**, *29*, 108833. [CrossRef]
77. Molnar, C. *Interpretable Machine Learning: A Guide for Making Black Box Models Explainable*; Lulu.com: London, UK, 2020.
78. Breiman, L.; Friedman, J.; Olshen, R.; Stone, C. *Classification and Regression Trees*; Biometrics, Wadsworth: Belmont, CA, USA, 1984.
79. Lei, X.; Chen, W.; Avand, M.; Janizadeh, S.; Kariminejad, N.; Shahabi, H.; Costache, R.; Shahabi, H.; Shirzadi, A.; Mosavi, A. GIS-Based Machine Learning Algorithms for Gully Erosion Susceptibility Mapping in a Semi-Arid Region of Iran. *Remote Sens.* **2020**, *12*, 2478. [CrossRef]
80. Rodriguez-Galiano, V.F.; Ghimire, B.; Rogan, J.; Chica-Olmo, M.; Rigol-Sanchez, J.P. An assessment of the effectiveness of a random forest classifier for land-cover classification. *ISPRS J. Photogramm. Remote Sens.* **2012**, *67*, 93–104. [CrossRef]
81. Pourghasemi, H.R.; Yousefi, S.; Kornejady, A.; Cerdà, A. Comparison of different machine learning methods for debris flow susceptibility mapping: A case study in Sichuan Province, China. *Geosci. Front.* **2020**, *11*, 2207–2219. [CrossRef]
82. Conoscenti, C.; Agnesi, V.; Angileri, S.E.; Cappadonia, C.; Rotigliano, E.; Schillaci, C. Comparison and ranking of different modelling techniques for gully erosion susceptibility mapping: A case study from southern Sicily, Italy. *Land Degrad. Dev.* **2021**, *32*, 4001–4017.
83. Jiang, C.; Fan, W.; Yu, N.; Liu, E. Spatial modeling of gully head erosion on the Loess plateau using a certainty factor and random forest model. *Sci. Total Environ.* **2021**, *783*, 147040. [CrossRef]
84. Gayen, A.; Pourghasemi, H.R.; Saha, S.; Keesstra, S.; Bai, S. Gully erosion susceptibility assessment and management of hazard-prone areas in India using different machine learning algorithms. *Sci. Total Environ.* **2019**, *668*, 124–138. [CrossRef] [PubMed]
85. Pham, Q.B.; Mukherjee, K.; Norouzi, A.; Linh, N.T.T.; Janizadeh, S.; Ahmadi, K.; Cerdà, A.; Doan, T.N.C.; Anh, D.T. Head-cut gully erosion susceptibility modeling based on ensemble random forest with oblique decision trees in Fareghan watershed, Iran. *Geomat. Nat. Hazards Risk* **2020**, *11*, 2385–2410. [CrossRef]

86. Montgomery, D.R.; Dietrich, W.E. Runoff generation in a steep, soil-mantled landscape. *Water Resour. Res.* **2002**, *38*, 1168. [CrossRef]
87. Wang, F.; Sahana, M.; Pahlevanzadeh, B.; Pal, S.C.; Shit, P.K.; Piran, M.J.; Janizadeh, S.; Band, S.S.; Mosavi, A. Applying different resampling strategies in machine learning models to predict head-cut gully erosion susceptibility. *Alex. Eng. J.* **2021**, *60*, 5813–5829. [CrossRef]
88. Roy, J.; Saha, S. Integration of artificial intelligence with meta classifiers for the gully erosion susceptibility assessment in Hinglo river basin, Eastern India. *Adv. Space Res.* **2021**, *67*, 316–333. [CrossRef]
89. Mohebzadeh, H.; Biswas, A.; Rudra, R.; Daggupati, P. Machine Learning Techniques for Gully Erosion Susceptibility Mapping: A Review. *Geosciences* **2022**, *12*, 429. [CrossRef]
90. Amiri, M.; Pourghasemi, H.R.; Ghanbarian, G.A.; Afzali, S.F. Assessment of the importance of gully erosion effective factors using Boruta algorithm and its spatial modeling and mapping using three machine learning algorithms. *Geoderma* **2019**, *340*, 55–69. [CrossRef]
91. Garosi, Y.; Sheklabadi, M.; Conoscenti, C.; Pourghasemi, H.R.; Van Oost, K. Assessing the performance of GIS-based machine learning models with different accuracy measures for determining susceptibility to gully erosion. *Sci. Total Environ.* **2019**, *664*, 1117–1132. [CrossRef]
92. Rahmati, O.; Tahmasebipour, N.; Haghizadeh, A.; Pourghasemi, H.R.; Feizizadeh, B. Evaluation of different machine learning models for predicting and mapping the susceptibility of gully erosion. *Geomorphology* **2017**, *298*, 118–137. [CrossRef]
93. Yang, A.; Wang, C.; Pang, G.; Long, Y.; Wang, L.; Cruse, R.M.; Yang, Q. Gully Erosion Susceptibility Mapping in Highly Complex Terrain Using Machine Learning Models. *ISPRS Int. J. Geo-Inf.* **2021**, *10*, 680. [CrossRef]
94. Angileri, S.E.; Conoscenti, C.; Hochschild, V.; Märker, M.; Rotigliano, E.; Agnesi, V. Water erosion susceptibility mapping by applying stochastic gradient treeboost to the Imera Meridionale river basin (Sicily, Italy). *Geomorphology* **2016**, *262*, 61–76. [CrossRef]
95. Capra, A.; Di Stefano, C.; Ferro, V.; Scicolone, B. Morphological characteristics of ephemeral gullies in Sicily, south Italy. *Landform Anal.* **2011**, *17*, 27–32.
96. Karydas, C.G.; Panagos, P. Towards an Assessment of the Ephemeral Gully Erosion Potential in Greece Using Google Earth. *Water* **2020**, *12*, 603. [CrossRef]
97. Vanwalleghem, T.; Bork, H.R.; Poesen, J.; Schmidtchen, G.; Dotterweich, M.; Nachtergaele, J.; Bork, H.; Deckers, J.; Brüsch, B.; Bungeneers, J.; et al. Rapid development and infilling of a buried gully under cropland, central Belgium. *Catena* **2005**, *63*, 221–243. [CrossRef]